Exploring ubiquitin and ISG15 biology with chemical tools

Gan, J.

Chapter 6.

Chemical improvement and cellular validation of OTUB2 inhibitors provides evidence for novel OTUB2 (auto-)regulatory mechanisms

Jin Gan, Jelle de Vries, Hans van Dam, Jimmy J.L.L.Akkermans, Rayman T. N. Tjokrodirijo, George M. C. Janssen, Robbert Q. Kim, David A. Vargas, Vito Pol, David A. Pérez Berrocal, Rudi Fasan, Peter A. van Veelen, Jacques Neefjes, Aysegul Sapmaz, Paul P. Geurink1, Huib Ovaa

Manuscript in preparation

ABSTRACT

Ubiquitin thioesterase OTUB2, a cysteine protease from the ovarian tumor (OTU) deubiquitinase superfamily is associated with enhanced expression during tumor progression and metastasis. Development of potent and specific OTUB2 inhibitors is therefore supposed to be therapeutically meaningful. Here, we describe an improved OTUB2 inhibitor, LN5P45, which is developed through lead optimization of the original compound OTUB2-COV1. The complete and high-resolution co-crystal structure of OTUB2 bound with LN5P45 explains the atomic details of inhibitor binding. Utilizing LN5P45 as a research tool, we found that OTUB2 lysine 31 is ubiquitinated upon the inhibitor treatment, and that ubiquitinated OTUB2 is degraded by the ubiquitin-proteasome system. Besides ubiquitination, we also detected increased OTUB2 mRNA levels upon inhibitor treatment. Thus, this work contributes to a deeper understanding of OTUB2 regulation at both post-translational protein modification and mRNA expression. Moreover, our findings provide novel insights for the design of future OTUB2-related therapeutics.

INTRODUCTION

Ubiquitination is an essential post-translational protein modification in many cellular processes. Ubiquitin generally modifies target proteins through lysine residues, and occasionally on cysteine, serine and threonine residues, which is catalyzed by sequential E1, E2 and E3 enzymes [1-3]. Protein ubiquitination either serves for cellular signalling, or target substrates for proteasomal degradation [4]. Deubiquitinases (DUBs) can reverse this process by removing conjugated ubiquitin from substrates [5]. A tightly regulated balance between ubiquitinating and deubiquitinating processes is critical for cellular homeostasis and dynamics. Post-translational modification of DUBs, including phosphorylation, ubiquitination, SUMOylation, acetylation *etc*, can further fine-tune these processes [6].

OTU domain-containing ubiquitin aldehyde-binding protein 2 (OTUB2) is a cysteine DUB [7]. Recent research revealed that elevated OTUB2 expression correlates with tumorigenesis and metastasis. OTUB2 can promote tumorigenic progression of non-small cell lung cancer (NSCLC) cells through deubiquitination of U2AF2, stimulation of Warburg effect, and activation of AKT/mTOR signaling [8]. Moreover, OTUB2 has been identified as a cancer stemness and metastasis-promoting factor that deubiquitinates YAP/TAZ proteins in breast cancer cells, whereby poly-SUMOylation on OTUB2 lysine 233 mediates the interaction with YAP/TAZ [9]. These studies demonstrate that development of OTUB2-specific inhibitors is potentially beneficial for cancer therapies.

Previous electrophile fragment screening enabled identification of the first OTUB2 inhibitor, OTUB2-COV1. However, the biological application of this compound is limited by its mild potency, and its improvement was restricted due to the imperfect co-crystal structure of the OTUB2-inhibitor complex and unknown absolute stereochemistry of the inhibitor [10]. Here we report the development of better OTUB2 inhibitors through optimization of the original OTUB2-COV1 inhibitor with respect to its stereochemistry and aromatic ring substituents. The complete and high-resolution co-crystal structure provides good insight into the atomic details behind the improved inhibitor potency. Utilizing the best inhibitor LN5P45 as a research tool, we unexpectedly found that OTUB2

lysine 31 is ubiquitinated after treatment with OTUB2 inhibitors, and that this ubiquitinated OTUB2 can be degraded by the ubiquitin-proteasome system. Besides ubiquitination, we also uncovered increased OTUB2 mRNA level upon inhibitor treatment.

RESULTS

OTUB2 inhibitor optimization

Previously, we showed that the chloroacethydrazide containing molecule COV-1 (Compound **1**, Figure 1, Table 1) can efficiently and DUB-selectively inhibit OTUB2 in both cell lysates and living cells [10]. Mass spectrometry analysis and X-ray crystallography showed that the inhibitor forms an irreversible, covalent bond with the OTUB2 active site cysteine, thereby substituting the chloride. However, the cocrystal structure revealed little information on the positioning and interactions of the cyclopropane moiety as no clear density was obtained. To further optimize the inhibitory properties of this compound, we first turned our attention to the stereochemistry of the substituents on the cyclopropane moiety, as the exact nature of the stereocenters in COV-1 were unknown. COV-1 is synthesized in two or three steps from 2-phenylcyclopropane-1-carboxylate **11** or its methyl or ethyl ester derivatives **12** and **13** as shown in Scheme 1.

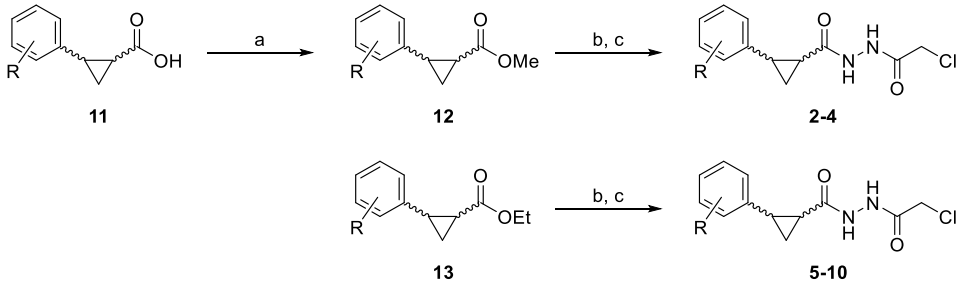

Scheme 1. General synthesis of arylcyclopropyl chloroacethydrazide OTUB2 inhibitors. Stereochemistry and R are defined as shown in Table 1. Reagents and conditions: (a) 2M TMS-diazomethane in Et_2O; (b) hydrazine hydrate, MeOH, 60 °C; (c) chloroacetylchloride, Et_3N, DCM.

Compound	Ar	C1	C2	IC_{50} (µM)	k_{inact}/K_I ($M^{-1}s^{-1}$)
1 (COV-1)	Ph	unknown		15.4*	n.d.
2 (LN4P43)	Ph	Mix (1R,2R) and (1S,2S)		14.1	n.d.
3 (LN4P44)	Ph	Mix (1R,2S) and (1S,2R)		>100	n.d.
4 (LN4P45)	Ph	S	R	>100	n.d.
5 (LN4P66)	Ph	R	R	13.6	4.8
6 (LN4P67)	Ph	S	S	6.8	14.7
7 (LN5P44)	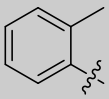	S	S	43.0	1.5
8 (LN5P45)	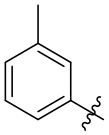	S	S	2.3	45.7
9 (LN5P46)	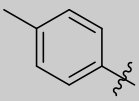	S	S	12.4	6.5
10 (LN5P47)	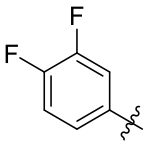	S	S	10.1	8.5

Table 2. Overview of the stereochemistry and substituents of the compounds along with the inhibition values.

The stereochemistry in the final product originates from the stereochemical nature of the starting compound and does not change during the course of the synthesis. We acquired three commercially available stereoisomers of 2-phenylcyclopropane-1-carboxylate (**11**): a racemic mixture of the *trans*-only isomers, a racemic mixture of the *cis*-only isomers, and the chirally pure *cis* isomer (1S,2R) from which compounds **2-4** were synthesized (Figure 1A, Table 1). The inhibitory potency of these compounds was assessed in a biochemical OTUB2 enzymatic activity assay using the fluorogenic substrate ubiquitin-rhodamine-morpholine (UbRhoMP) [11]. Recombinant human OTUB2 [12] was incubated with a serial dilution of each compound for 2 hours before the addition of the substrate and subsequent recording of the fluorescence intensity over time. The percentage inhibition was calculated from the activity curves and normalized to the positive (10 mM *N*-ethylmaleimide, 100% inhibition) and negative (DMSO, 0% inhibition) controls. The inhibition was plotted against the compound concentration from which the IC_{50} values were calculated (Figure 1B, Table 1). From the results it became indisputably clear that only the compounds having the *trans* configuration inhibit OTUB2. Virtually no inhibition was observed for the *cis* configuration compounds **3** and **4**, whereas the IC_{50} value for compound **2** is nearly identical to that of compound **1**. Hence we concluded that compound **1** most likely has the *trans* configuration and that this is required for OTUB2 inhibition.

Next, we examined whether one of the *trans* stereoisomers would be favoured. The required chirally pure *trans* ethyl 2-phenylcyclopropane-1-carboxylate (**13**) starting compounds could be obtained using the chemoenzymatic stereoselective olefin cyclopropanation developed by the Fasan lab [13, 14]. Both stereoisomers were produced with this method, and from these compounds the corresponding chloroacethydrazides compound **5** (1R,2R) and **6** (1S,2S) were prepared and tested for OTUB inhibition (Table 1). From the obtained IC_{50} values (Figure 1B, Table 1) it becomes apparent that, although both stereoisomers inhibit OTUB2, compound **6** having the (1S,2S) configuration is the most potent one with an IC_{50} value of 6.8 µM, which makes it about twice as potent compared to the initial COV-1 compound.

After having determined the (1S,2S) configuration as the preferred stereoisomer we turned our attention to the aromatic ring substituents to further improve the compounds potency. The above mentioned chemoenzymatic stereoselective olefin cyclopropanation was applied in the synthesis of the (1S,2S) chirally pure compounds **7-10** having a methyl of fluorine substituent at different positions on the aromatic ring. The compounds were tested for their OTUB2 inhibitory potency using the same assay (Figure 1C, Table 1). Introduction of a methyl group at the *para* position (compound **9**) or a 3,4-difluoride (compound **10**) did not affect the IC_{50} much, but the *ortho*-methyl group had a detrimental effect (compound **7**). Notably, introducing a *meta*-methyl group (compound **8**) increased the inhibitory potency, resulting in an IC_{50} of 2.3 µM. Since these compounds are all covalent, irreversible inhibitors [10], the IC_{50} is dependent on the incubation time. In order to get a better estimate of their respective inhibitory capacity, independent of incubation time, we determined the k_{inact}/K_I values of compounds **5-10** by pre-mixing the compounds with substrate before adding OTUB2. The obtained values corroborate well with the IC_{50} values (Table 1).

To assess the ability of compounds **5-10** to modify OTUB2 in cells, we performed gel-based competitive activity-based protein profiling (ABPP) in similar assays as described previously for COV-1 [10, 15]. HEK293T cells overexpressing GFP-OTUB2 were incubated with DMSO or increasing concentrations of the OTUB2 inhibitors, followed by

cell lysis and co-incubation with fluorescently tagged ubiquitin-based activity-based probe (Rho-Ub-PA) [15]. This probe covalently labels the active site cysteine of DUBs that are not already blocked by inhibitors. The labeled DUBs were next resolved by SDS-PAGE and imaged by fluorescence scanning. Based on comparison to a DMSO control sample, we could conclude that all inhibitors were engaged with cellular OTUB2 in a dose-dependent manner, indicating that all inhibitors can penetrate the cell membrane well (Figure 1D). Compound **6** (LN4P67), compound **8** (LN5P45), and compound **10** (LN5P47) displayed clear inhibition from 10 µM, corresponding very well to their *in vitro* IC_{50} values (Table 1). More importantly, compound **8** (also named LN5P45, Figure 2A) outperforms the other inhibitors both *in vitro* and in cells. We therefore decided to continue with this compound.

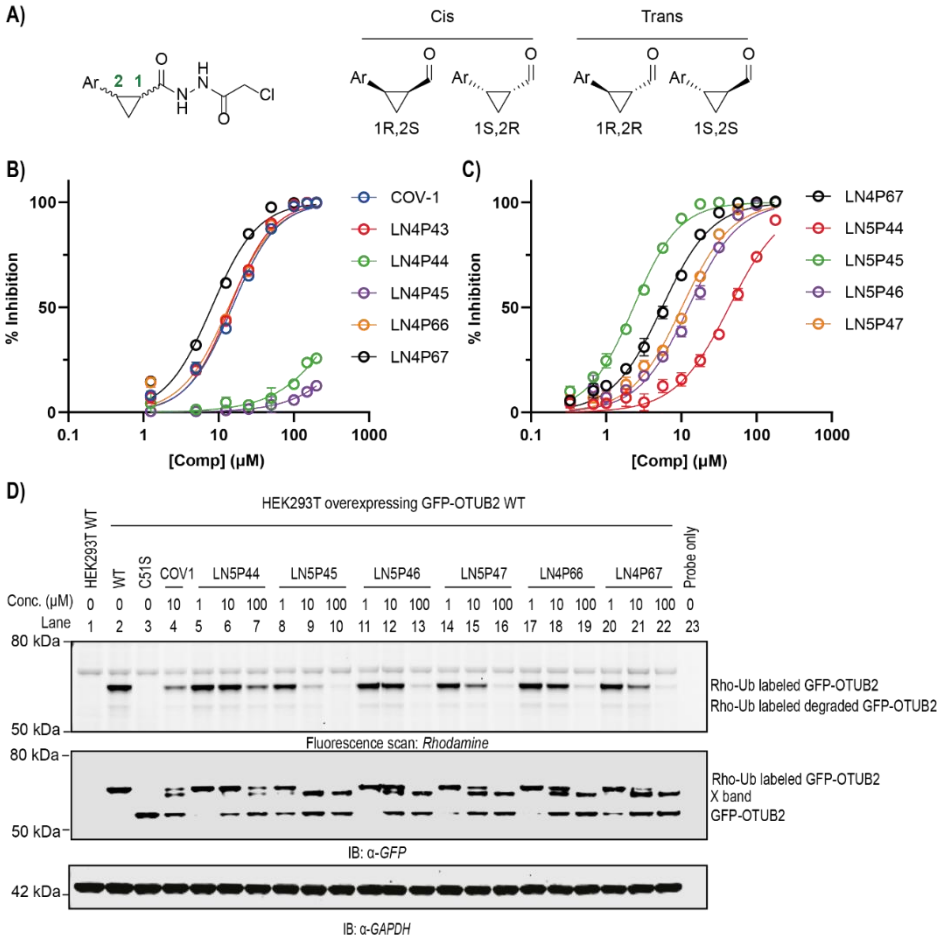

Figure 1. Optimization of OTUB2 inhibitors. (A) General structure of the OTUB2 inhibitors used in this study. A clarification of the different stereochemistry is shown. (B, C) Inhibition curves of the indicated compounds against OTUB2. Compounds were

incubated with OTUB2 prior to addition of the Ub-Rhodamine substrate and fluorescence read-out. The percentage inhibition was calculated from the activity curves and normalized to the positive (10 mM *N-ethylmaleimide*, 100% inhibition) and negative (DMSO, 0% inhibition) controls. The inhibition was plotted against the compound concentration from which the IC_{50} values (see Table 1) were calculated. (D) Inhibition of GFP-OTUB2 by the indicated compounds in HEK293T cells (see Supplementary figure 1 for full images). GFP-OTUB2 (WT or catalytic dead mutant C51S) was transiently transfected in HEK293T cells. After 24 hours, cells were treated with indicated inhibitors at indicated concentrations for 4 hours. Cell lysates were incubated with Rho-Ub-PA probe, and subjected to SDS-PAGE, gel fluorescence scanning, and immunoblotting. Top: fluorescence scan of Rho-Ub-PA probe labelled DUBs. Middle: anti-GFP immunoblot data corresponding to probe labelled and unlabeled GFP-OTUB2 (An extra band was annotated as "X band", see results in Figure 4). Bottom: anti-GAPDH immunoblot data validating equal loading of each sample.

Determination of the cocrystal structure of OTUB2 in complex with LN5P45

We next set out to evaluate the binding mode of LN5P45 within the OTUB2 active site. LC-MS analysis of OTUB2 before and after reaction with LN5P45 confirmed the formation of a covalent complex by showing a mass difference of 230 Da, which corresponds to a substitution reaction at the chloride (Figure 2B and Supplementary Figure 2). To further confirm the binding to the active site cysteine and to obtain information on the structural aspects of the interactions we solved the cocrystal structure of OTUB2 in complex with LN5P45 at 1.22Å resolution. In contrast to the cocrystal structure of the OTUB2-COV-1 complex (PDB 5QIO), in our OTUB2-LN5P45 structure we were able to obtain a clear density for the cyclopropyl-phenyl moiety, which is likely due to the fact that LN5P45 has the defined (1S,2S) configuration (Figure 2A,C). The phenyl ring moiety points outside the protein toward the solvent and has as such no obvious interactions. Its orientation however could explain our earlier observation that only the compounds with the *trans* substituted cyclopropane ring (compounds **5-10**) and not the *cis*-linked ones (compounds **3** and **4**) inhibited OTUB2. The latter situation would likely result into a conformational clash of the phenyl group with the protein. This could also explain the finding that the *ortho*-methyl-substituted compound **7** showed diminished inhibition. The *trans* orientation on the other hand nicely positions the inhibitor inside the small groove leading to the active site. From the cocrystal structure it does not become clear why the *meta*-methyl is the preferred substitution over the *para*-substitution. The binding of the acethydrazide part with the OTUB2 active site compared well with earlier findings from the PDB 5QIO structure (Figure 2D). Active site Cys51 is covalently bound (distance is 1.7Å) to the acetamide-Cα and the acetamide carbonyl occupies the oxyanion hole formed by the backbone NH of residues Asp48, Gly49 (note that this is misannotated as Arg49 in the PDB 5QIO structure), Asn50, and Cys51 and the sidechain carboxylate of Asp48. The carbonyl directly attached to the cyclopropane ring interacts with the side chain of His224 through a hydrogen bond, and the Glu174 side chain carboxylate also forms hydrogen bonds with both of the hydrazide amines.

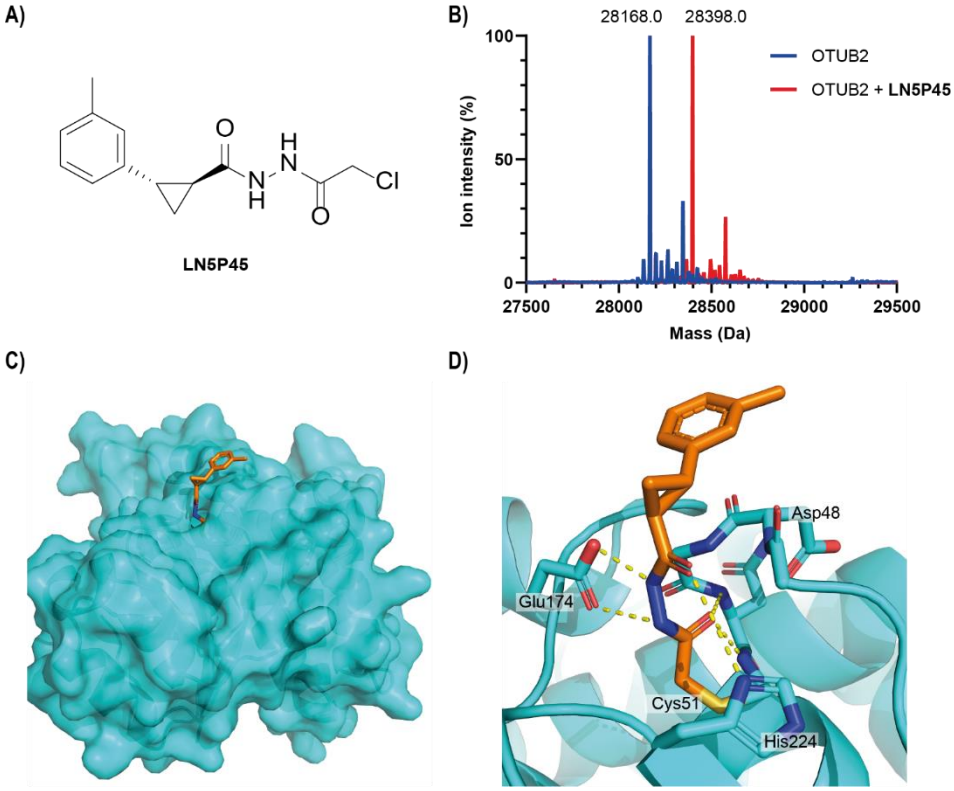

Figure 2. Characterization of the interactions between OTUB2 and inhibitor LN5P45. (A) Chemical structure of LN5P45. (B) Deconvoluted mass spectra of OTUB2 before (blue) and after (red) reaction with LN5P45. (C) Surface structure of human OTUB2 (azure surface) in complex with LN5P45 (brown sticks) showing that the trans substituted cyclopropane ring of LN5P45 points phenyl ring outside the protein toward the solvent. (D) Cartoon structure of the binding pockets of LN5P45 (brown sticks) in active site of OTUB2 (azure ribbons). The key residues interacting with LN5P45 are shown as sticks, hydrogen bonds are shown in yellow dashed lines.

LN5P45 selectively engages endogenous OTUB2 over other ubiquitin machinery components

To validate that LN5P45 also can engage with endogenous OTUB2, we used the bone-metastatic (BM) derivative of breast cancer cell line MDA-MB-231, which was reported to express relatively high levels of OTUB2 compared to other breast cancer lines [9]. Because of the lack of a good antibody that selectively recognizes endogenous OTUB2, siRNA-mediated depletion of endogenous OTUB2 was performed as control to confirm OTUB2 labeling with our Rho-Ub-PA probe. This enabled identification of a specific protein band (around 35 kDa) that was substantially reduced in the OTUB2 depleted sample (Figure 3A,B). The observed molecular weight of this labeled protein matched with the expected molecular weight of Rho-Ub-PA-labeled OTUB2 (OTUB2 27.2 kDa + 8 kDa Ub probe). Moreover, upon incubation of living BM MDA-MB-231 cells with 10 or 20

µM LN5P45 for 4 hours, this Rho-Ub-PA-labeled OTUB2 band almost disappeared compared to the DMSO control sample (Figure 3A). Since none of the other Rho-Ub-PA labeled bands were affected by the OTUB2 inhibitor, this result indicates that LN5P45 can specifically inhibit endogenous OTUB2.

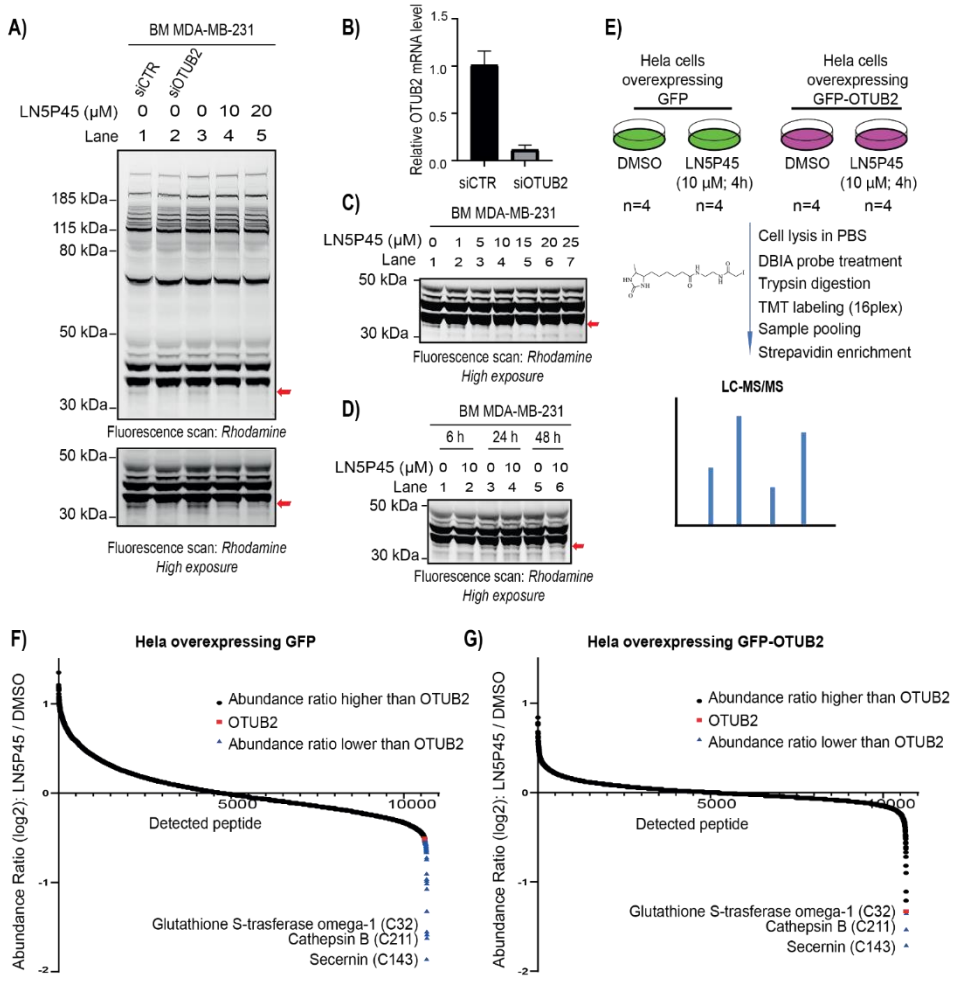

Figure 3. LN5P45 engages endogenous OTUB2, and is selective for OTUB2 over other ubiquitin machinery components. (A) Gel-based fluorescence labeling of endogenous OTUB2 in bone-metastatic (BM) MDA-MB-231 cells (see Supplementary figure 3A for instant-blue stained loading control). BM MDA-MB-231 cells were treated with the indicated concentrations of LN5P45 for 4 hours, followed by cell lysis, incubation with Rho-Ub-PA DUB probe, SDS-PAGE, and gel fluorescence scanning. (B) Real time RT–PCR for Otub2 transcripts in BM MDA-MB-231 cells treated with OTUB2 siRNA for 72 hours (Right). Bars represent means ± S.E.M with three samples in each group. Data are representative of four independently performed experiments. (C, D) BM MDA-MB-231 cells were treated with the indicated concentrations of LN5P45 for 4 hours (C), or 10 µM LN5P45 for the indicated time (D), followed by cell lysis, incubation with Rho-Ub-PA

DUB probe, SDS-PAGE, and gel fluorescence scanning; representative of n=3 independent experiments. (see Supplementary figure 3B,C for full image of fluorescence scan and instant-blue stained loading control of C, D). (E) Schematic representation of the streamlined cysteine activity-based protein profiling (SLC-ABPP) shown in (F) and (G). (F, G) Waterfall plots of the 10,670 cysteine sites modified by the DBIA probe in LN5P45- versus DMSO- treated HeLa cells overexpressing GFP (F) or GFP-OTUB2 (G).

To evaluate the potency and stability of OTUB2 inhibition with LN5P45 in BM MDA-MB-231 cells, Rho-Ub-PA labeling was performed after treatment with increasing concentrations and for different amounts of time. When treated for 4 hours, complete inhibition was observed from 10 μM on (Figure 3C). However, this inhibition was hardly observed after 24 or 48 hours of incubation (Figure 3D).

The Rho-Ub-PA profile obtained for BM MDA-MB-231 cells suggested that OTUB2 is the only DUB target of LN5P45 in these cells (Figure 3A,C; Supplementary Figure 3B). To further investigate LN5P45's selectivity throughout the proteome, we performed recently developed streamlined cysteine activity-based protein profiling (SLC-ABPP, a variant of rdTOP-ABPP) to determine its cysteine targets [16]. We first examined BM MDA-MB-231 cells, but unfortunately were unable to detect OTUB2, which might be due to low abundance of OTUB2 in the lysates. We subsequently analysed HeLa cells over-expressing either GFP or GFP-OTUB2 WT (Figure 3E). OTUB2 (C51) was detectable in the HeLa cells overexpressing GFP. This might be due to the fact that the GFP and GFP-OTUB2 WT TMT-labeled samples were pooled for LC-MS/MS detection. The OTUB2 inhibition by LN5P45 in the GFP cells was mild, ranking 68th out 10,670 peptides (Figure 3F, Supplementary table 1). However, in the GFP-OTUB2 expressing cells, overall OTUB2 inhibition became very significant (Figure 3G, Supplementary table 2). This suggests that the protein abundance affects the quantification accuracy. In the SLC-ABPP experiments, binding of the desthiobiotin iodoacetamide (DBIA) probe to several proteins not involved in ubiquitination was also inhibited in the presence of LN5P45, e.g., for Secernin-3 (C143) Cathepsin B (C211), and Glutathione S-transferase omega-1(C32). In addition, DBIA probe-binding to USP15 (C264) and USP8 (C809) was found to be mildly inhibited in Hela cells overexpressing GFP, but the affected cysteines are not part of the active sites of these DUBs. Taken together, these findings affirmed that LN5P45 engages cellular OTUB2 and is selective for OTUB2 over other DBIA probe-binding ubiquitin machinery components at 10 μM.

LN5P45 treatment results in ubiquitination of OTUB2 on lysine 31

Interestingly, the western blot analysis of GFP-OTUB2 in Figure 1D had shown an additional GFP-OTUB2 band upon inhibitor treatment (annotated as "X band" in Figure 1D). Since this might represent a modified version of OTUB2 induced by the inhibitor, we further examined its appearance and its nature. Comparison of the effects of two different OTUB2 inhibitors in living HEK293T cells versus cell lysates showed that (i) a weak X band can already be detected in the DMSO-treated GTP-OTUB2 WT expressing cells , and that (ii) in living cells X band is increased by inhibitor treatment, and also by disruption of the OTUB2 catalytic activity through genetic inactivation (C51S) (Figure 4A). Moreover, Rho-Ub-PA probe labeling did not affect the abundance of X band in the inhibitors-treated living cells, and its appearance was independent of Rho-Ub-PA probe labeling (Figure 4A).

Of note, the slower migrating GFP-OTUB2 X band was not dependent on the presence of the OTUB2-fused GFP tag, as a similar slower migrating band was detected with a Flag antibody in cells ectopically expressing Flag-HA tagged OTUB2 (Figure 4B). We therefore hypothesized that modification of exogenously expressed OTUB2 in cells is induced upon OTUB2 inhibitor treatment.

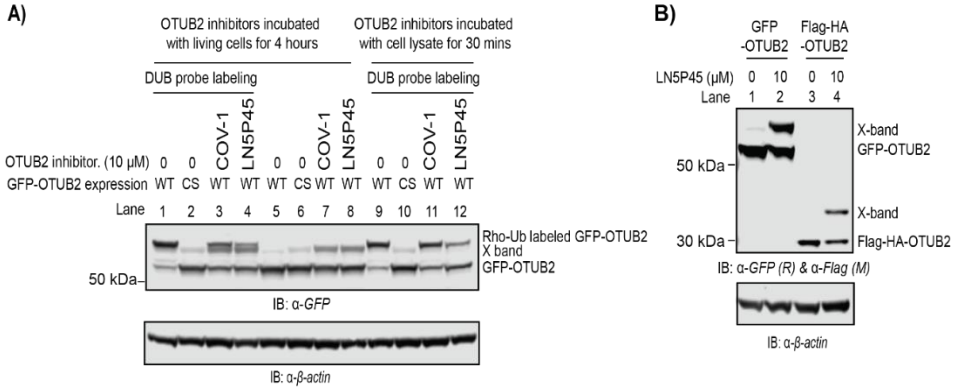

Figure 4. GFP- and Flag-HA-OTUB2 "X-band" mobility shifts upon treatment with LN5P45 inhibitor. (A) HEK293T cells overexpressing GFP-OTUB2 WT or C51S mutant were untreated or treated with 10 μM OTUB2 inhibitors for 4 hours, and after lysis labeled with Rho-Ub-PA probe (lane 1-4), or unlabeled (lane 5-8). Cell lysates from HEK293T cells overexpressing GFP-OTUB2 WT or C51S mutant were incubated with 10 μM OTUB2 inhibitors for 30 min as indicated, and next labelled with Rho-Ub-PA probe (lane 9-12). Top: anti-GFP immunoblot data corresponding to GFP-OTUB2. Middle: fluorescence scan of Rho-Ub-PA probe labelled DUBs. Bottom: anti- β-actin immunoblot data corresponding to equal loading of each sample. (B) HEK293T cells overexpressing GFP-OTUB2 WT or Flag-HA-OTUB2 WT were treated with 10 μM OTUB2 inhibitors for 4 hours before harvesting, then lysed and subjected to immunoblotting. α-GFP (Rabbit) and α-Flag (Mouse) mixed together for primary antibody incubation. Anti-rabbit 800 and anti-mouse 680 mixed together for secondary antibody incubation.

To elucidate the nature of this modification, we used GFP trap beads and SDS-PAGE to enrich the band X protein in the samples from HEK293T cells overexpressing GFP-OTUB2 WT (10 μM LN5P45 treated for 4 hours vs non-treated), excised the protein bands surrounding the X band area, and subjected the samples to protein mass spectrometry analysis (Figure 5A). The analysis revealed highly abundant ubiquitin peptides at the exact X band location (Figure 5B). This finding was confirmed by anti-ubiquitin immunoblot analysis of the pulled-down GFP-OTUB2 samples, which indicates that band X corresponds to mono-ubiquitinated GFP-OTUB2 while the less abundant slower migrating bands represent ubiquitinated forms with additional modifications (Figure 5C). Consistent with the data above, a low level of ubiquitination on GFP-OTUB2 can already be detected in non-treated cells, but OTUB2 inactivation by inhibitor treatment or, to a lesser extent, active site mutation enhances the mono-ubiquitination level (Figure 5C, D, Figure 4A). When OTUB2 ubiquitination was examined by HA-Ub overexpression, poly-ubiquitination bands on GFP-OTUB2 after inhibitor treatment were observed as well (Supplementary Figure 4A).

We next set out to identify which amino acid(s) is/are ubiquitinated in GFP-OTUB2. Although peptide sequencing by mass spectrometry failed to locate the specific modification site, it helped us to exclude several lysines. OTUB2 K12, K31, K37, K44, K46 and K221 were possible sites, and we therefore generated single lysine to arginine mutants of GFP-OTUB2 for each of these sites. Analysis in HEK293T cells showed that only K31R mutation resulted in loss of the mono-ubiquitination band upon OTUB2 inhibitor treatment, and that mono-ubiquitination of the catalytic inactive mutant C51S was not further increased by the inhibitor either (Figure 5E). Moreover, K31R mutation also disrupted the strong LN5P45-induced poly-ubiquitination bands detected in the pulled-down GFP-OTUB2 under HA-Ub overexpression conditions (Supplementary Figure 4B). Altogether, these data prove lysine 31 to be the site responsible for inhibitor induced ubiquitination on OTUB2.

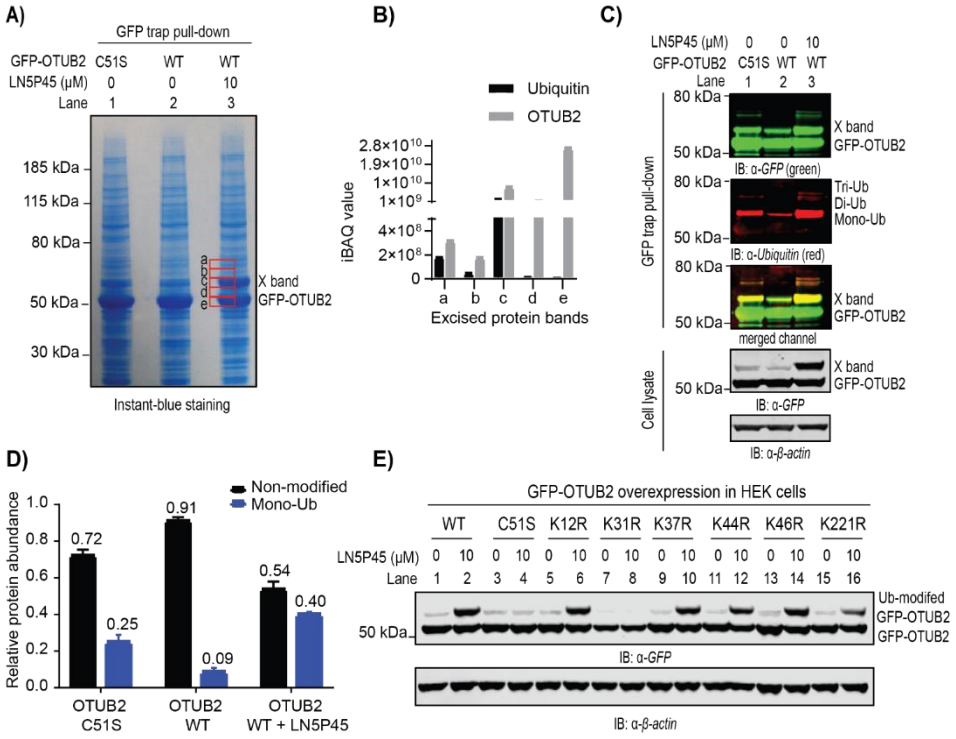

Figure 5. OTUB2 is monoubiquitinated on lysine 31 upon inhibitor treatment. (A) Instant-blue staining of SDS-PAGE of the indicated GFP-trap-pulled-down proteins. GFP-OTUB2 WT or C51S were transfected into HEK293T cells as indicated. 24 h post transfection, cells were incubated with DMSO or 10 μM LN5P45 for 4 hours as indicated. GFP-OTUB2 was enriched by GFP trap beads, subjected to SDS-PAGE separation, and bands a-e were excised for mass spectrometry analysis. (B) Label-free quantification of the amount of ubiquitin and OTUB2 in the excised protein bands. (C) Ubiquitination on GFP-OTUB2 is confirmed by immunoblotting of the GFP-trap enriched proteins with anti-ubiquitin

antibody. (D) Quantification of the non-modified and mono-Ub modified GFP-OTUB2 amounts in Figure 4C; the immunoblot intensity (based on α-GFP IB signal) was quantified by Image J software. The total GFP signal was regarded as 1. The percentage was averaged from n=3 independent experiments. (E) Lysine to arginine point mutation analysis of OTUB2 identifies lysine 31 as critical for OTUB2 mono-ubiquitination. The indicated GFP-OTUB2 mutants were exogenously expressed in HEK293T cells, the cells were treated with or without LN5P45 at 10 μM for 4 hours, and cell lysates were immunoblotted with GFP antibody.

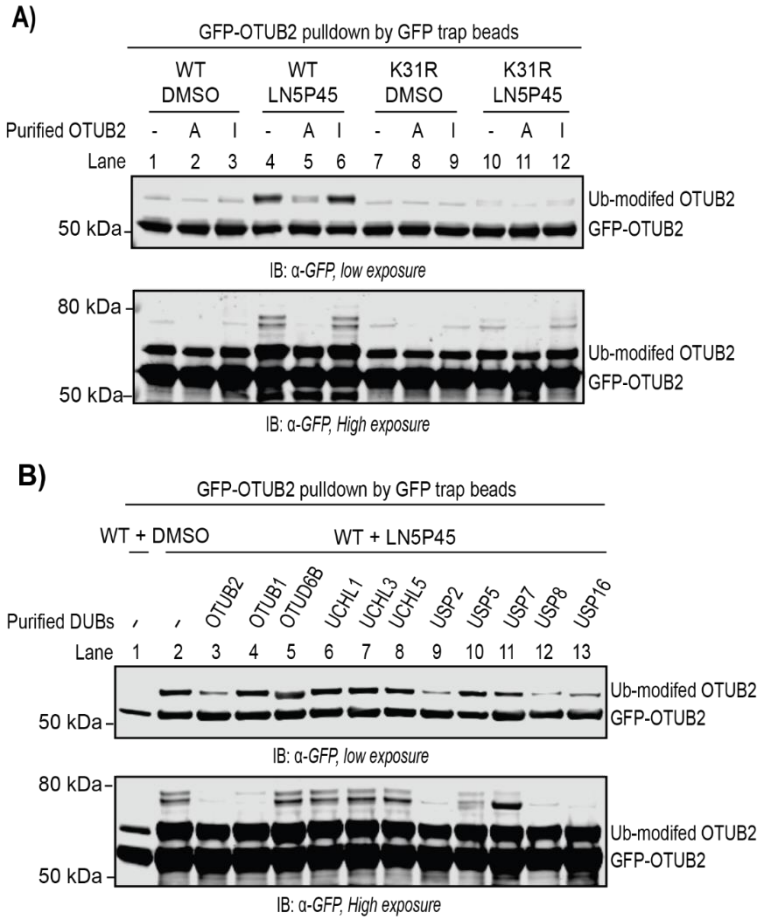

Figure 6. *In vitro* deubiquitination of ubiquitinated OTUB2**.** (A) Ubiquitinated OTUB2 is cleaved by purified OTUB2 *in vitro*. GFP-OTUB2 WT or K31R constructs were transfected into HEK293T cells as indicated. At 24 h post transfection, cells were incubated with DMSO or LN5P45 at 10 μM for 4 hours before harvesting as indicated. After GFP trap pull-down the proteins were used as substrates for *in vitro* cleavage assays. Purified OTUB2 proteins were pre-treated with or without LN5P45 (inhibitory conc. 100 μM) for 10 min. before adding into the on-beads digestion. A: purified OTUB2 is active; I: purified OTUB2 is inactivated by LN5P45 inhibitor preincubation treatment. (B) *In vitro* ubiquitinated OTUB2 cleavage assay with a panel of purified DUBs. GFP-OTUB2 WT

proteins, immunoprecipitated (IP) from HEK293T cells (LN5P45 treated for 4 hours at 10 μM vs non-treated), were used as substrates for *in vitro* cleavage assay. OTUB2, OTUB1, GST-OTUD6B, UCHL1, UCHL3 and UCHL5 were added at final concentration of 2.5 μM; USP2, USP5, USP7, USP8 and USP16 full-length protein were added with a total amount of 1 μg.

Since OTUB2 is a deubiquitinase and its inactivation enhances its monoubiquitination (Figure 4A, Figure 5C, D), we wanted to know whether OTUB2 can cleave off ubiquitin from itself. We, therefore, performed *in vitro* deubiquitination assays with GFP-OTUB2 WT and K31R proteins purified from cells that were either untreated, or treated with LN5P45 at 10μM for 4 hours. Upon GFP trap pull-down, the proteins served as the substrates for cleavage assays with purified active or inactive OTUB2. These assays showed that purified active OTUB2 can indeed efficiently reverse the ubiquitination modifications of OTUB2 (Figure 6A, lane 4-6). Interestingly, OTUB2 K31R still has a weak modification band upon inhibitor treatment, which might be due to potential "hopping" of ubiquitin conjugation in alternative lysine residues, but the level is much lower than detected for WT (Figure 6A, lane 10 vs lane 7). To examine whether this ubiquitination cleavage was specific for OTUB2, we tested a panel of DUBs from the OTU, UCH and USP families, including purified OTUB1, OTUD6B, UCHL1, UCHL3, UCHL5, USP2, USP5, USP7, USP8 and USP16. OTUB1, a close homologue of OTUB2, specifically cleaves lysine 48-linked Ub chains [7, 17], did not affect the major monoUb band of OTUB2, but did reduce the slower migrating forms, indicating the slower migrating forms might be lysine 48-linked Ub chains. The promiscuous DUBs USP2 and USP8 could cleave all of the Ub forms as efficiently as OTUB2, as did USP16, albeit less efficient towards the monoUb form (Figure 6B). These *in vitro* deubiquitination assays demonstrate that OTUB2 efficiently deubiquitinates itself, while some other DUBs (USP2, USP8, USP16) show efficient cleavage *in vitro* as well.

In summary, the above data demonstrate that OTUB2 is ubiquitinated via lysine 31, that inactivation of OTUB2 by catalytic site mutation or inhibitor treatment leads to elevated ubiquitination, and that active OTUB2 can counteract this ubiquitination process, at least *in vitro*.

LN5P45 treatment accelerates OTUB2 degradation through ubiquitin-proteasome pathway

We subsequently analysed whether inhibitor treatment and increased ubiquitination affects the stability of OTUB2 in cells. We first examined the degradation rate of exogenously expressed GFP-OTUB2 WT in HEK293T cells in a Cycloheximide (CHX) chase experiment (Figure 7A, B). CHX treatment blocks eukaryotic cytosolic translation by impairing ribosomal translocation [18, 19]. The amount of GFP-OTUB2 WT decreased following the addition of CHX in a time-dependent manner (lane 5-8 vs lane 1-4), and the addition of OTUB2 inhibitor LN5P45 accelerated the degradation of both monoubiquitinated GFP-OTUB2 (lane 13-16 vs lane 9-12) and total GFP-OTUB2 (unmodified GFP-OTUB2 + monoubiquitinated GFP-OTUB2) (lane 13-16 vs lane 5-8). These data suggested that OTUB2 inhibitor treatment enhances the turnover of exogenously expressed OTUB2.

Next, we examined whether changes in proteasome activity influenced OTUB2 turnover. For this, HEK293T cells exogenously expressing GFP-OTUB2 WT or K31R were treated with the proteasome inhibitor MG132, or the activators PD169316 or Win 62577 [20]

(Figure 7C, D). Compared with the DMSO-treated control group (lane 1 and 2), the protein amount of monoubiquitinated GFP-OTUB2 WT and total GFP-OTUB2 WT increased upon treatment with the inhibitor MG132 (lane 3 and 4), and decreased substantially after addition of activators PD169316 (lane 5 and 6) and Win 62577 (lane 7 and 8). On the other hand, GFP-OTUB2 K31R was insensitive to proteasome activity modulation (lane 9-16). This indicates that the inhibitor-induced OTUB2 ubiquitination affects its turnover through the proteasome pathway.

LN5P45 treatment elevates endogenous OTUB2 transcription level

It is quite common that cells evolve feedback reactivation of target proteins or signaling pathways as a key mechanism of adaptive resistance to inhibitors [21, 22]. For example, catalytic proteasome inhibition concertedly upregulates the expression of proteasomal subunits [23] and induces the formation of alternative proteasome complexes [24], which may compensate for the reduced proteasome activity. To check whether OTUB2 has a similar feedback mechanism, we performed real-time PCR (RT-PCR) analysis to investigate putative changes in the OTUB2 mRNA level upon treatment of BM MDA-MB-231 cells with LN5P45 (Figure 8A). Interestingly, OTUB2 mRNA level was elevated following the inhibitor treatment for 24 hours and 48 hours. This indicates that cells might start feedback reactivation of OTUB2 upon the inhibitor treatment.

As the inhibition of endogenous OTUB2 by LN5P45 is short-lived in BM MDA-MB-231 cells (Figure 3C), we reasoned that the inhibition might be prolonged if de novo synthesis of OTUB2 is interrupted in cells. Therefore, we examined the inhibition of endogenous OTUB2 by LN5P45 in the presence or absence of CHX for the last 6 hours (Figure 8B, Supplementary Figure 3D). Indeed, the OTUB2 inhibition after 24 hours of LN5P45 was restored when the new OTUB2 synthesis was blocked by CHX treatment (lane 7-8 vs lane 3-4); also OTUB2 inhibition after 6 hours seemed improved with the addition of CHX (lane 5-6 vs lane 1-2), suggesting that BM MDA-MB-231 cells adapt itself to upregulate OTUB2 expression to resistant OTUB2 inhibition.

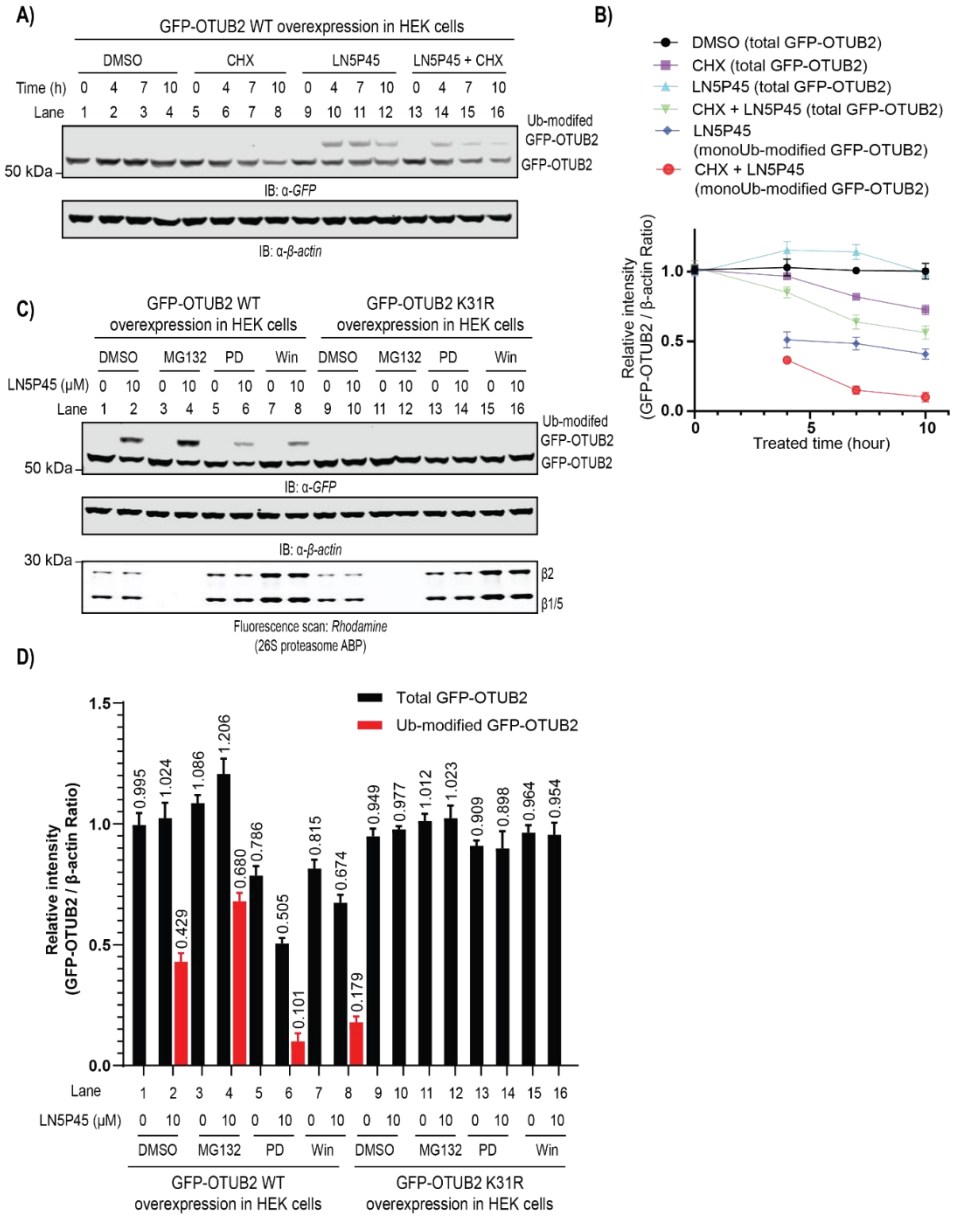

Figure 7. LN5P45 treatment accelerates OTUB2 degradation through the ubiquitin-proteasome pathway. (A) Cycloheximide (CHX) chase analysis of overexpressed GFP-OTUB2 WT degradation in HEK293T cells. GFP-OTUB2 construct was transiently transfected into HEK293T cells for 24 hours, CHX (final conc. 100 μg/ml) and LN5P45 (final conc. 10 μM) were added for the indicated times. Representative data from n = 3 biological replicates. (B) The protein band intensities of the immunoblot results from (A) were quantified and analyzed by ImageJ. n = 3 biological replicates. Total GFP-OTUB2 includes both monoubiquitinated and unmodified GFP-OTUB2. (C) GFP-OTUB2 WT and

K31R protein level changes in HEK293T cells upon modulation of proteasome activity. GFP-OTUB2 WT or K31R constructs were transiently transfected into HEK293T cells for 24 hours, proteasome activators PD (PD1619316) and Win (WIN 62577) were added at final concentration of 5μM along with the transfection mixture (incubation for 24 hours), LN5P45 (final conc. 10 μM) and proteasome inhibitor MG132 (final conc. 5 μM) were added for 4 hours before harvesting the cells. Cell lysates were subjected to immunoblot against GFP and β-actin. Top: anti-GFP immunoblot data corresponding to GFP-OTUB2 and monoubiquitinated GFP-OTUB2. Middle: anti-β-actin immunoblot data corresponding to equal loading of each sample. Bottom: fluorescence scan of 26S proteasome probe corresponding to proteasome activity. Representative data from n = 3 biological replicates. (D) The protein band intensity of the immunoblot results from (A) were quantified and analyzed by ImageJ. n = 3 biological replicates.

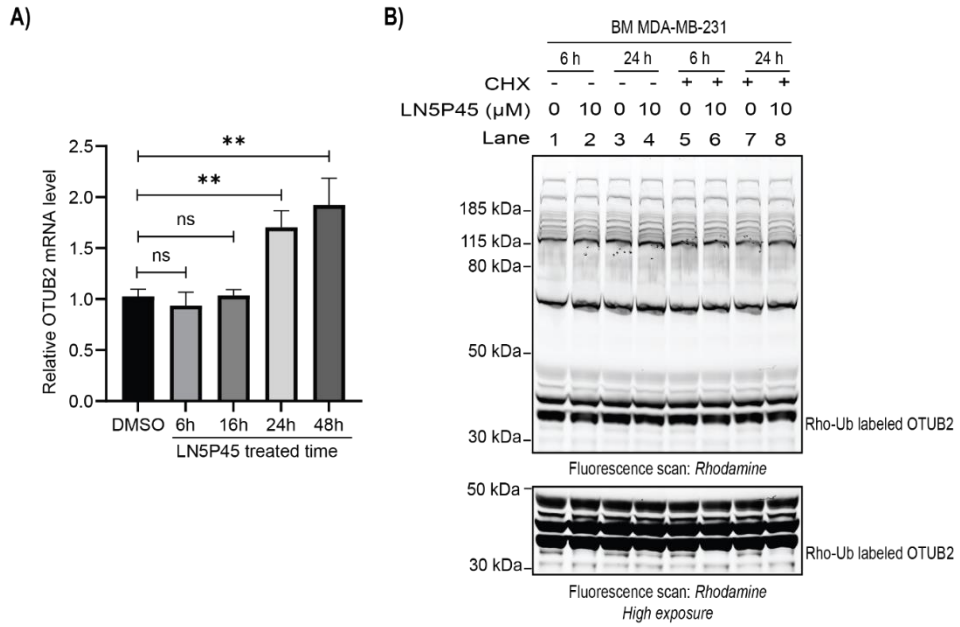

Figure 8. LN5P45 treatment elevates endogenous OTUB2 transcription level. (A) Quantitative RT–PCR for *Otub2* transcripts in BM MDA-MB-231 cells treated with LN5P45 (final conc. 10 μM) for the indicated times. Control cells were treated with DMSO for 48 hours. Bars represent means ± S.E.M with three samples in each group. (B) Gel-based fluorescence labeling of endogenous OTUB2 in bone-metastatic (BM) MDA-MB-231 cells (see Supplementary figure 3D for instant-blue stained loading control). Cells were treated with LN5P45 (final conc. 10 μM) for the indicated time; CHX (final conc. 100 μg/ml) was added 6 hours before cell harvesting. Cell lysates were incubated with Rhodamine-tagged Ub-PA DUB probe, subjected to SDS-PAGE and fluorescence scanning. Representative data from n = 3 biological replicates.

DISCUSSION

DUBs play key roles in diverse biological processes by regulating the cellular activity and abundance of critical proteins and maintaining the dynamic state of the cellular ubiquitome. Especially in the last decades, outstanding advances have been made in the understanding of DUB structure, function, regulation and disease involvement [25, 26]. The development of potent and specific DUB inhibitors has yielded many drug-like molecules for therapeutic intervention in numerous diseases [27-29], and also provided versatile tools to further investigate their cellular localizations [11], biological functions [30], and biochemical mechanisms [31].

In this study, we developed the improved covalent OTUB2 inhibitor LN5P45 through optimization of the original OTUB2-COV1 inhibitor by addressing absolute stereochemistry and aromatic ring substituents. We were able to determine the preferred absolute stereochemistry to be 1S,S2 and the LN5P45-OTUB2 cocrystal structure explained the molecular details of the inhibitor binding mode. The costructure also revealed that the aromatic moiety points outside the protein. For future inhibitor optimizations it could be worthwhile to introduce more hydrophilic residues at the phenyl ring to accommodate for its solvent-exposed nature. Our substituent analysis revealed that the *meta* position on the aromatic ring is the best site to introduce modifications. This opens the way to install fluorescent/affinity tags or E3 ligase ligands in order to create OTUB2-specific activity-based probes or PROTACS respectively.

In the target engagement experiments in cells, we found OTUB2 to be ubiquitinated at lysine 31 upon inhibitor treatment. It is quite common for DUBs to be ubiquitinated, which can regulate their function, localization, or stability. For example, monoubiquitination of OTUB1 - primarily at lysine 59 and 109 - is critical for OTUB1 to suppress UbcH5 and induce P53 [32], and the DUB activity of Ataxin-3 and JosD1 can be enhanced through the ubiquitination of lys 117 on Ataxin-3 [33, 34], and lys136 on JosD1 [35]. As opposed to activation, the enzymatic activity of UCHL1 is restricted by monoubiquitination of lysine residues near the active site [36]. In addition to these activity changes, the subcellular localization of BAP1 is regulated by multi-monoubiquitination within its NLS region [37]. USP30 is ubiquitinated by parkin for proteasome degradation [38]. The results on OTUB2 presented here indicate that the inhibitor-induced ubiquitination of OTUB2 is associated with ubiquitin-proteasome degradation. However, monoubiquitination is the primary form of OTUB2 ubiquitination, which is generally regarded as a regulatory modification for protein interaction, activity and localization [1]. Thus it is in future studies needed to investigate putative inhibitor-induced changes in OTUB2's interactions with other proteins, and changes in function and subcellular localization, e.g., through comparison of OTUB2 WT and K31R. Moreover, as UBE2O catalyzes the multi-monoubiquitination of BAP1 [37], UbcH5 monoubiquitinates OTUB1 [32], ubiquitin E3 ligase Ro52 ubiquitinates USP4 [39], and TRIM27 ubiquitinates USP7 [40], it would be interesting to investigate the E2 / E3 enzymes involved in the OTUB2 ubiquitination process.

Another interesting question is why OTUB2 is ubiquitinated upon inhibitor treatment. All of the OTUB2 inhibitors with different stereoisomers and aromatic ring substituents can induce the mono-ubiquitination band (Figure 1D), and the intensity of the band is proportional to the potency of inhibitors, so it is unlikely to be a molecular glue or PROTAC effect of the inhibitors that induces the proximity between OTUB2 and ubiquitin E2 / E3 enzymes. It is known that inhibitor binding can promote structural changes and

degradation of its target proteins [41]. However, the crystal structures of OTUB2 (PDB: 1TFF) and inhibitor-bound OTUB2 are nearly identical, so it is unlikely to be an effect of conformational change induced by inhibitor treatment. Albeit LN5P45 has several off-targets in cells, these are unlikely to affect cellular ubiquitination. Untreated OTUB2 could also be mono-ubiquitinated at a low level, but OTUB2 inactivation by either active site mutation or inhibitor treatment enhances the ubiquitination level (Figure 4A, Figure 5C), and ubiquitinated OTUB2 could be cleaved by recombinant OTUB2 *in vitro* (Figure 6A). These results suggest an OTUB2 auto-deubiquitinating mechanism to keep itself sufficiently stable in cells, which is a common mechanism utilized by many other DUBs, like BAP1 [37], USP25 [42], USP4 [39], and USP6 [43]. The addition of OTUB2 inhibitors would then disrupts OTUB2 self-cleavage. However, this auto-deubiquitinating hypothesis needs more intracellular experiments and similar data for endogenous OTUB2.

Besides OTUB2 ubiquitination, we also found increased OTUB2 mRNA levels upon LN5P45 treatment. It may represent a feedback mechanism to counteract the inhibition by synthesizing de novo protein to make up for the enzymatic activity loss of OTUB2. Unfortunately, we lack a good antibody to assess the ubiquitination of endogenous OTUB2 and its turnover in immunoblots. Endogenously tagging OTUB2 with a detection tag using CRISPR /Cas9 knock-in technology [44] would be a useful strategy to overcome the antibody problem. Regardless, it is not unexpected that cells have mechanisms to overcome OTUB2 small-molecule inhibition by promoting inhibited OTUB2 to be ubiquitinated and degraded by the proteasome, and to trigger new OTUB2 production.

From the perspective of drug development, it is apparent that inhibition of OTUB2 activity may not be sufficient. PROTAC-mediated degradation, and inhibition of OTUB2 at the transcriptional or translational level would be beneficial for the development of OTUB2-targeted therapeutics.

ACKNOWLEDGMENTS

This work was supported by Oncode and a VICI grant (no. 724.013.002) from The Netherlands Organization for Scientific Research (NWO) to H.O. Grant (no. ICI00026) from Institute for chemical immunology to A.S. The authors thank Patrick Voskamp from the Crystallization Facility (Leiden Institute of Chemistry) and Diamond Light Source for beamtime (proposal mx19800); specifically staff of beamline I04-1 for assistance with data collection.

1. Komander, D. and M. Rape, *The ubiquitin code.* Annu Rev Biochem, 2012. **81**: p. 203-29.
2. Hershko, A. and A. Ciechanover, *The ubiquitin system.* Annu Rev Biochem, 1998. **67**: p. 425-79.
3. McDowell, G.S. and A. Philpott, *Non-canonical ubiquitylation: mechanisms and consequences.* Int J Biochem Cell Biol, 2013. **45**(8): p. 1833-42.
4. Swatek, K.N. and D. Komander, *Ubiquitin modifications.* Cell Res, 2016. **26**(4): p. 399-422.
5. Mevissen, T.E.T. and D. Komander, *Mechanisms of Deubiquitinase Specificity and Regulation.* Annu Rev Biochem, 2017. **86**: p. 159-192.
6. Wang, Y. and F. Wang, *Post-Translational Modifications of Deubiquitinating Enzymes: Expanding the Ubiquitin Code.* Front Pharmacol, 2021. **12**: p. 685011.
7. Balakirev, M.Y., et al., *Otubains: a new family of cysteine proteases in the ubiquitin pathway.* EMBO Rep, 2003. **4**(5): p. 517-22.
8. Li, J., et al., *OTUB2 stabilizes U2AF2 to promote the Warburg effect and tumorigenesis via the AKT/mTOR signaling pathway in non-small cell lung cancer.* Theranostics, 2019. **9**(1): p. 179-195.
9. Zhang, Z., et al., *OTUB2 Promotes Cancer Metastasis via Hippo-Independent Activation of YAP and TAZ.* Mol Cell, 2019. **73**(1): p. 7-21 e7.
10. Resnick, E., et al., *Rapid Covalent-Probe Discovery by Electrophile-Fragment Screening.* J Am Chem Soc, 2019. **141**(22): p. 8951-8968.
11. Kooij, R., et al., *Small-Molecule Activity-Based Probe for Monitoring Ubiquitin C-Terminal Hydrolase L1 (UCHL1) Activity in Live Cells and Zebrafish Embryos.* J Am Chem Soc, 2020. **142**(39): p. 16825-16841.
12. Mons, E., et al., *Exploring the Versatility of the Covalent Thiol-Alkyne Reaction with Substituted Propargyl Warheads: A Deciding Role for the Cysteine Protease.* J Am Chem Soc, 2021. **143**(17): p. 6423-6433.
13. Bordeaux, M., V. Tyagi, and R. Fasan, *Highly diastereoselective and enantioselective olefin cyclopropanation using engineered myoglobin-based catalysts.* Angew Chem Int Ed Engl, 2015. **54**(6): p. 1744-8.
14. Sreenilayam, G., et al., *Stereoselective olefin cyclopropanation under aerobic conditions with an artificial enzyme incorporating an iron-chlorin e6 cofactor.* ACS Catal, 2017. **7**(11): p. 7629-7633.
15. Ekkebus, R., et al., *On terminal alkynes that can react with active-site cysteine nucleophiles in proteases.* J Am Chem Soc, 2013. **135**(8): p. 2867-70.
16. Kuljanin, M., et al., *Reimagining high-throughput profiling of reactive cysteines for cell-based screening of large electrophile libraries.* Nat Biotechnol, 2021. **39**(5): p. 630-641.

17. Mevissen, T.E.T., et al., *OTU deubiquitinases reveal mechanisms of linkage specificity and enable ubiquitin chain restriction analysis.* Cell, 2013. **154**(1): p. 169-184.

18. Ennis, H.L. and M. Lubin, *CYCLOHEXIMIDE: ASPECTS OF INHIBITION OF PROTEIN SYNTHESIS IN MAMMALIAN CELLS.* Science, 1964. **146**(3650): p. 1474-6.

19. Buchanan, B.W., et al., *Cycloheximide Chase Analysis of Protein Degradation in Saccharomyces cerevisiae.* Journal of visualized experiments : JoVE, 2016(110): p. 53975.

20. Leestemaker, Y., et al., *Proteasome Activation by Small Molecules.* Cell Chem Biol, 2017. **24**(6): p. 725-736 e7.

21. Ryan, M.B., et al., *Vertical Pathway Inhibition Overcomes Adaptive Feedback Resistance to KRAS(G12C) Inhibition.* Clin Cancer Res, 2020. **26**(7): p. 1633-1643.

22. Park, S.M., et al., *Feedback analysis identifies a combination target for overcoming adaptive resistance to targeted cancer therapy.* Oncogene, 2020. **39**(19): p. 3803-3820.

23. Meiners, S., et al., *Inhibition of proteasome activity induces concerted expression of proteasome genes and de novo formation of Mammalian proteasomes.* J Biol Chem, 2003. **278**(24): p. 21517-25.

24. Welk, V., et al., *Inhibition of Proteasome Activity Induces Formation of Alternative Proteasome Complexes.* J Biol Chem, 2016. **291**(25): p. 13147-59.

25. Harrigan, J.A., et al., *Deubiquitylating enzymes and drug discovery: emerging opportunities.* Nat Rev Drug Discov, 2018. **17**(1): p. 57-78.

26. Clague, M.J., S. Urbé, and D. Komander, *Breaking the chains: deubiquitylating enzyme specificity begets function.* Nature Reviews Molecular Cell Biology, 2019. **20**(6): p. 338-352.

27. Rowinsky, E.K., et al., *Phase 1 study of the protein deubiquitinase inhibitor VLX1570 in patients with relapsed and/or refractory multiple myeloma.* 2020. **38**(5): p. 1448-1453.

28. Schauer, N.J., et al., *Advances in Discovering Deubiquitinating Enzyme (DUB) Inhibitors.* Journal of Medicinal Chemistry, 2019.

29. Yuan, T., et al., *Inhibition of Ubiquitin-Specific Proteases as a Novel Anticancer Therapeutic Strategy.* Front Pharmacol, 2018. **9**: p. 1080.

30. Clancy, A., et al., *The deubiquitylase USP9X controls ribosomal stalling.* J Cell Biol, 2021. **220**(3).

31. Wang, Y., et al., *Small molecule inhibitors reveal allosteric regulation of USP14 via steric blockade.* Cell Res, 2018. **28**(12): p. 1186-1194.

32. Li, Y., et al., *Monoubiquitination is critical for ovarian tumor domain-containing ubiquitin aldehyde binding protein 1 (Otub1) to suppress UbcH5 enzyme and stabilize p53 protein.* J Biol Chem, 2014. **289**(8): p. 5097-108.

33. Todi, S.V., et al., *Activity and Cellular Functions of the Deubiquitinating Enzyme and Polyglutamine Disease Protein Ataxin-3 Are Regulated by Ubiquitination at Lysine 117*.* Journal of Biological Chemistry, 2010. **285**(50): p. 39303-39313.

34. Todi, S.V., et al., *Ubiquitination directly enhances activity of the deubiquitinating enzyme ataxin-3.* The EMBO journal, 2009. **28**(4): p. 372-382.

35. Seki, T., et al., *JosD1, a membrane-targeted deubiquitinating enzyme, is activated by ubiquitination and regulates membrane dynamics, cell motility, and endocytosis.* The Journal of biological chemistry, 2013. **288**(24): p. 17145-17155.

36. Meray, R.K. and P.T. Lansbury, Jr., *Reversible monoubiquitination regulates the Parkinson disease-associated ubiquitin hydrolase UCH-L1.* J Biol Chem, 2007. **282**(14): p. 10567-75.

37. Mashtalir, N., et al., *Autodeubiquitination protects the tumor suppressor BAP1 from cytoplasmic sequestration mediated by the atypical ubiquitin ligase UBE2O.* Mol Cell, 2014. **54**(3): p. 392-406.

38. Bingol, B., et al., *The mitochondrial deubiquitinase USP30 opposes parkin-mediated mitophagy.* Nature, 2014. **510**(7505): p. 370-375.

39. Wada, K. and T. Kamitani, *UnpEL/Usp4 is ubiquitinated by Ro52 and deubiquitinated by itself.* Biochemical and Biophysical Research Communications, 2006. **342**(1): p. 253-258.

40. Zaman, M.M.-U., et al., *Ubiquitination-deubiquitination by the TRIM27-USP7 complex regulates tumor necrosis factor alpha-induced apoptosis.* Molecular and cellular biology, 2013. **33**(24): p. 4971-4984.

41. Campaner, E., et al., *A covalent PIN1 inhibitor selectively targets cancer cells by a dual mechanism of action.* Nat Commun, 2017. **8**: p. 15772.

42. Denuc, A., et al., *The UBA-UIM domains of the USP25 regulate the enzyme ubiquitination state and modulate substrate recognition.* PloS one, 2009. **4**(5): p. e5571-e5571.

43. Shen, C., et al., *Calcium/Calmodulin Regulates Ubiquitination of the Ubiquitin-specific Protease TRE17/USP6*.* Journal of Biological Chemistry, 2005. **280**(43): p. 35967-35973.

44. Koch, B., et al., *Generation and validation of homozygous fluorescent knock-in cells using CRISPR–Cas9 genome editing.* Nature Protocols, 2018. **13**(6): p. 1465-1487.

Supporting information

MATERIALS AND METHODS

Chemical synthesis of OTUB2 inhibitors

General

General reagents were purchased from Sigma-Aldrich, Biosolve, and Acros, and used as received. Solvents were purchased from Biosolve, Sigma-Aldrich and VWR and used as received. *Trans*-2-phenyl-1-cyclopropanecarboxylic acid (CAS number 939-90-2, article number QB-1747) and (1*R*,2*S*)-Rel-2-phenylcyclopropanecarboxylic acid (CAS number 939-89-9, article number QW-9456) were purchased from Combi-Blocks Inc. (*1S,2R*)-2-phenylcyclopropane-1-carboxylic acid (CAS number 23020-18-0, article number O33621) was purchased from Advanced ChemBlocks Inc.

(*S*,*S*)-ethyl-2-(3,4-difluorophenyl)cyclopropane-1-carboxylate, (*S*,*S*)-ethyl-2-(*p*-tolyl)cyclopropane-1-carboxylate, (*S*,*S*)-ethyl-2-(*m*-tolyl)cyclopropane-1-carboxylate, (*S*,*S*)-ethyl-2-(*o*-tolyl)cyclopropane-1-carboxylate, (*S*,*S*)-ethyl-2-phenylcyclopropane-1-carboxylate, (*R*,*R*)-ethyl-2-phenylcyclopropane-1-carboxylate were provided by the Fasan Lab.

Thin Layer Chromatography (TLC) was performed on Merck aluminium sheets (pre-coated with silica gel 60 F254). Compounds were visualized by UV absorption (254 nm) and by using a solution of $KMnO_4$ (7.5 g L^{-1}) and K_2CO_3 (50 g L^{-1}) in H_2O or a solution of ninhydrin (15 g L^{-1}) in 3% AcOH/EtOH v/v. Compounds (unless stated otherwise) were purified on a Büchi Sepacore automatic flash chromatography system X10/X50. The Büchi Sepacore system was equipped with two Büchi pump modules C-605, a Büchi control unit C-620, Büchi fraction collector C-660 and a Büchi UV Photometer C-640. The silica columns were purchased at GraceResolv™ and were packed with a grade of Davisil® silica. NMR spectra (^{1}H, ^{13}C) were recorded on a Bruker Ultrashield 300 MHz spectrometer at 298 K. Resonances are indicated with symbols 'd' (doublet), 'ddd' (double double doublet), 'dt' (double triplet), 's' (singlet), 't' (triplet) and 'm' (multiplet). Chemical shifts (δ) are given in ppm relative to $CDCl_3$, DMSO-d6 or CD_3OD as an internal standard and coupling constants (*J*) are quoted in hertz (Hz).

LC-MS measurements were performed on a LC-MS system equipped with a Waters Acquity H-Class UPLC system with an Extended λ Photodiode Array Detector (210-800 nm), an Acquity BEH C18 Column (130 Å, 1.7 µm, 2.1 mm x 50 mm) and a LCT-Premier ESI-Orthogonal Acceleration Time of Flight Mass Spectrometer.

Samples were run using 3 mobile phases: A = Purified deionized Water (Veolia - H_2O), B = Acetonitrile (UPLC grade - CH_3CN) and C = 44% H_2O, 44% CH_3CN, 12% Formic acid (UPLC grade – HCO_2H). Data processing was performed using Waters MassLynx Mass Spectrometry Software 4.1. UPLC-MS Program: flow rate = 0.5 mL/min, runtime = 3 min, column T = 40 °C, mass detection: 100–1500 Da. Gradient: Line C, provides a constant 4% of the total composition. Initial conditions 94% A, 2% B, 4% C. at 0.2 min. Composition gradually changes over 1.6 min, to 96 %B and 4% C at 1.80 min. This is kept untill 2.15 min before changing back to the original composition at 2.20 min and remains so untill the 3 min time mark.

General procedures:

(a) A solution of 2M TMS-diazomethane in Et_2O (4 eq.) was added dropwise in 15 minutes to a solution of the carboxylic acid in dry MeOH (ca. 0.3 M). After stirring at room temperature overnight TLC analysis indicated the reaction to be complete. The mixture was concentrated to dryness *in vacuo* at 40 °C and used as obtained in the next step.

(b) The methyl ester (or ethyl ester for the compounds obtained from the Fasan Lab) was dissolved in MeOH (ca. 0.06 – 0.7M). An excess of hydrazine monohydrate (10 – 50 eq.) was added and the mixture was stirred at 60 °C until the starting material had been consumed as indicated by TLC and/or LCMS analysis. The mixture was concentrated to dryness *in vacuo* at 40 °C and co-evaporated 3x with toluene. The obtained material was used in the next step without further purification.

(c) The crude hydrazide was taken up in DCM (ca. 0.01 – 0.05M). Et_3N (3 eq.) was added, followed by chloroacetylchloride (1.1 eq.) After TLC analysis indicated the reaction to be complete the mixture was diluted ca. 2x with DCM and washed with an equal amount of H_2O. The organic layer was dried ($MgSO_4$), filtered through a paper filter and adsorbed onto Celite. Purification was performed using a silica gel column with an ethyl acetate/heptane gradient as eluent after which the purest fractions were combined and concentrated *in vacuo* at 40 °C.

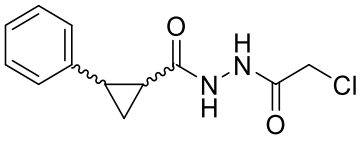

1:1 mix *trans* configuration

LN4P43 (2)

The compound was synthesized according to general procedures A, B and C starting from commercially available t*rans*-2-phenyl-1-cyclopropanecarboxylic acid and obtained as a white solid. Yield: 3 mg, 0.012 mmol, 11 % over 3 steps. ^{1}H NMR (300 MHz, DMSO-d_6) δ 10.28 (d, *J* = 14.1 Hz, 2H), 7.37 – 7.10 (m, 5H), 4.14 (s, 2H), 2.31 (ddd, *J* = 9.0, 6.3, 4.1 Hz, 1H), 1.96 (ddd, *J* = 8.3, 5.3, 4.1 Hz, 1H), 1.48 – 1.30 (m, 2H). ^{13}C NMR (75 MHz, DMSO-d_6) δ 170.49, 165.22, 141.00, 128.85, 126.62, 126.30, 41.33, 24.83, 24.31, 15.97.

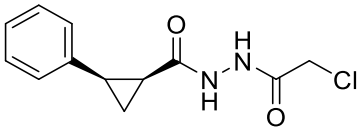

LN4P44 (3)

The compound was synthesized according to general procedures A, B and C starting from commercially available (1*R*,2*S*)-Rel-2-phenylcyclopropane-1-carboxylate and obtained as a white solid. Yield: 10 mg, 0.040 mmol, 28 % over 3 steps. ^{1}H NMR (300 MHz, Chloroform-*d*) δ 9.41 (d, *J* = 5.3 Hz, 1H), 8.93 (d, *J* = 5.1 Hz, 1H), 7.25 – 7.05 (m, 5H),

3.79 (s, 2H), 2.48 (q, *J* = 8.5 Hz, 1H), 1.89 (ddd, *J* = 9.0, 7.9, 5.5 Hz, 1H), 1.67 (dt, *J* = 7.6, 5.3 Hz, 1H), 1.30 (ddd, *J* = 8.8, 7.9, 5.0 Hz, 1H). ^{13}C NMR (75 MHz, Chloroform-*d*) δ 167.77, 163.00, 136.16, 129.26, 127.98, 126.74, 40.66, 25.91, 20.89, 10.95.

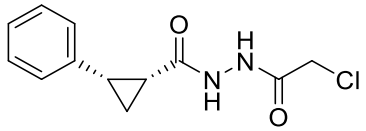

LN4P45 (4)

The compound was synthesized according to general procedures A, B and C starting from commercially available (1*S*,2*R*)-2-phenylcyclopropane-1-carboxylate and obtained as a white solid. Yield: 8 mg, 0.031 mmol, 24 % over 3 steps. ^{1}H NMR (300 MHz, Chloroform-*d*) δ 9.26 (d, *J* = 5.1 Hz, 1H), 8.80 (d, *J* = 4.9 Hz, 1H), 7.22 – 7.07 (m, 5H), 3.80 (d, *J* = 1.6 Hz, 2H), 2.49 (q, *J* = 8.5 Hz, 1H), 1.90 (ddd, *J* = 9.0, 7.9, 5.5 Hz, 1H), 1.69 (dt, *J* = 7.6, 5.3 Hz, 1H), 1.31 (ddd, *J* = 8.8, 7.9, 5.0 Hz, 1H). ^{13}C NMR (75 MHz, Chloroform-*d*) δ 167.85, 163.13, 136.10, 129.25, 128.00, 126.75, 40.67, 25.97, 21.04, 10.98.

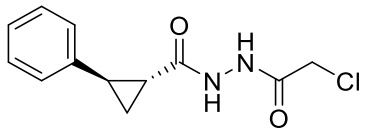

LN4P66 (5)

The compound was synthesized according to general procedures B and C starting from (*R*,*R*)-ethyl-2-phenylcyclopropane-1-carboxylate provided by Fasan Lab and obtained as a white solid. Yield: 12.3 mg, 0.049 mmol, 9 % over 2 steps. ^{1}H NMR (300 MHz, DMSO-d_6) δ 10.30 (d, *J* = 2.1 Hz, 1H), 10.25 (d, *J* = 2.1 Hz, 1H), 7.33 – 7.13 (m, 5H), 4.13 (s, 2H), 2.29 (ddd, *J* = 9.0, 6.3, 4.1 Hz, 1H), 1.94 (ddd, *J* = 8.3, 5.4, 4.1 Hz, 1H), 1.46 – 1.26 (m, 2H). ^{13}C NMR (75 MHz, DMSO-d_6) δ 170.47, 165.22, 141.01, 128.85, 126.61, 126.30, 41.32, 24.81, 24.32, 15.96.

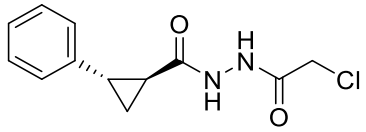

LN4P67 (6)

The compound was synthesized according to general procedures B and C starting (*S*,*S*)-ethyl-2-phenylcyclopropane-1-carboxylate provided by Fasan Lab and obtained as a white solid. Yield: 8.3 mg, 0.033 mmol, 6 % over 2 steps. ^{1}H NMR (300 MHz, DMSO-d_6) δ 10.30 (s, 1H), 10.25 (s, 1H), 7.36 – 7.25 (m, 2H), 7.24 – 7.12 (m, 3H), 4.13 (s, 2H), 2.29 (ddd, *J* = 8.9, 6.4, 4.2 Hz, 1H), 1.94 (ddd, *J* = 8.3, 5.4, 4.1 Hz, 1H), 1.39 (ddd, *J* = 9.2, 5.4,

4.1 Hz, 1H), 1.35 – 1.30 (m, 1H). ^{13}C NMR (75 MHz, DMSO-d_6) δ 170.47, 165.22, 141.01, 128.85, 126.61, 126.29, 41.32, 24.81, 24.32, 15.96.

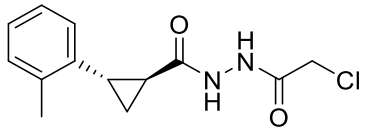

LN5P44 (7)

The compound was synthesized according to general procedures B and C starting from (*S*,*S*)-ethyl-2-(*o*-tolyl)cyclopropane-1-carboxylate provided by Fasan Lab and obtained as a white solid. Yield: 8.2 mg, 0.031 mmol, 13 % over 2 steps. ^{1}H NMR (300 MHz, DMSO-d_6) δ 10.33 (d, *J* = 2.1 Hz, 1H), 10.25 (d, *J* = 2.2 Hz, 1H), 7.22 – 7.07 (m, 3H), 7.07 – 6.98 (m, 1H), 4.13 (s, 2H), 2.34 – 2.24 (m, 4H), 1.79 – 1.70 (m, 1H), 1.37 – 1.31 (m, 1H). ^{13}C NMR (75 MHz, DMSO-d_6) δ 171.01, 165.23, 138.60, 137.86, 130.02, 126.85, 126.36, 125.90, 41.34, 23.18, 22.32, 19.69, 13.68.

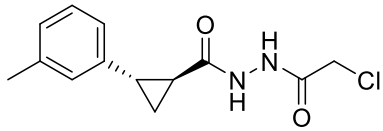

LN5P45 (8)

The compound was synthesized according to general procedures B and C starting from (*S*,*S*)-ethyl-2-(*m*-tolyl)cyclopropane-1-carboxylate provided by Fasan Lab and obtained as a white solid. Yield: 6.1 mg, 0.023 mmol, 10 % over 2 steps. ^{1}H NMR (300 MHz, DMSO-d_6) δ 10.24 (s, 2H), 7.17 (t, *J* = 48.7, 7.5 Hz, 1H), 7.06 – 6.88 (m, 3H), 4.13 (s, 2H), 2.30 – 2.20 (m, 4H), 1.96 – 1.88 (m, 1H), 1.42 – 1.33 (m, 1H), 1.33 – 1.29 (m, 1H). ^{13}C NMR (75 MHz, DMSO-d_6) δ 170.52, 165.21, 140.88, 137.95, 128.74, 127.28, 126.96, 123.41, 41.32, 24.80, 24.17, 21.44, 15.81.

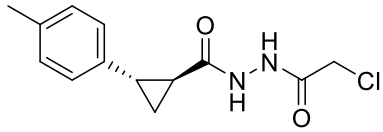

LN5P46 (9)

The compound was synthesized according to general procedures B and C starting from (*S*,*S*)-ethyl-2-(*p*-tolyl)cyclopropane-1-carboxylate provided by Fasan Lab and obtained as a white solid. Yield: 2.2 mg, 0.0082 mmol, 3 % over 2 steps. ^{1}H NMR (300 MHz, DMSO-d_6) δ 10.25 (s, 2H), 7.10 (d, *J* = 7.7 Hz, 2H), 7.03 (d, *J* = 8.2 Hz, 2H), 4.13 (s, 2H), 2.30 – 2.21 (m, 4H), 1.89 (ddd, *J* = 8.3, 5.3, 4.1 Hz, 1H), 1.36 (ddd, *J* = 9.2, 5.3, 4.0 Hz, 1H), 1.31

– 1.26 (m, 1H). ^{13}C NMR (75 MHz, DMSO-d_6) δ 170.56, 165.21, 137.88, 135.63, 129.40, 126.22, 41.32, 24.56, 24.08, 21.05, 15.83.

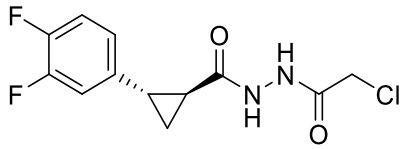

LN5P47 (10)

The compound was synthesized according to general procedures B and C starting from (*S*,*S*)-ethyl-2-(3,4-difluorophenyl)cyclopropane-1-carboxylate provided by Fasan Lab and obtained as a white solid. Yield: 6.5 mg, 0.023 mmol, 20 % over 2 steps. ^{1}H NMR (300 MHz, DMSO-d_6) δ 10.30 (d, J = 2.1 Hz, 1H), 10.25 (d, J = 2.2 Hz, 1H), 7.42 – 7.30 (m, 1H), 7.31 – 7.20 (m, 1H), 7.07 – 6.99 (m, 1H), 4.12 (s, 2H), 2.33 (ddd, J = 8.8, 6.5, 4.1 Hz, 1H), 1.98 – 1.89 (m, 1H), 1.43 – 1.33 (m, 2H). ^{13}C NMR (75 MHz, DMSO-d_6) δ 170.10, 165.19, 151.49, 150.02, 148.25, 146.79, 139.12, 123.21, 117.77, 115.29, 41.30, 24.56, 23.94, 16.10.

Synthesis and purification of the DBIA probe

The chemical synthesis and purification of the DBIA probe was performed the same as published before [1].

Ubiquitin substrate in vitro cleavage assays

The assays were performed in "nonbinding surface flat bottom low flange" black 384-well plates (Corning) at room temperature in a buffer containing 50 mM Tris·HCl, 100 mM NaCl, pH 7.6, 2.0 mM cysteine, 1 mg/mL 3-[(3-cholamidopropyl)-dimethylammonio]propanesulfonic acid (CHAPS), and 0.5 mg/mL γ-globulins from bovine blood (BGG). Each well had a final volume of 20.4 µL. The compounds were dissolved in 10 mM DMSO stocks, and appropriate volumes were transferred to the empty plates using a Labcyte Echo acoustic dispenser. A DMSO back-fill was performed to obtain equal volumes of DMSO (400 µL) in each well. *N*-ethylmaleimide (NEM, 10 mM) was used a positive control (100% inhibition) and DMSO as negative control (0% inhibition). A 10 µL portion of buffer was added, and the plate was vigorously shaken for 20s. Next, 5 µL of OTUB2 (full length) was added to a final concentration of 25 nM followed by incubation for 120 min. A 5 µL portion of the substrate (UbRhoMP) was added (final concentration 400 nM), and the increase in fluorescence over time was recorded using a BMG Labtech PHERAstar plate reader (excitation 487 nm, emission 535 nm). The initial enzyme velocities were calculated from the slopes, normalized to the positive and negative controls, and plotted against the inhibitor concentrations (in M) using the built-in equation "[inhibitor] vs response − variable slope (four parameters), least-squares fit" with constraints "Bottom = 0" and "Top = 100" in GraphPad Prism 7 software to obtain the IC_{50} values.

In case of the k_{inact}/K_I determinations the order of OTUB2 and substrate addition was reversed and no incubation time was used. All data fitting and calculations were done using GraphPad Prism 7 software. The fluorescence intensities were plotted against time (in

seconds) after a baseline correction using the DMSO control for each inhibitor concentration. The data were fitted to the equation FI = $(v_i/k_{obs})[1-e^{-k(obs)t}]$

Covalent Complex Formation Mass Spectrometry Analysis

Samples of 1.4 μM OTUB2 in 70 μL buffer containing 50 mM Tris·HCl, 100 mM NaCl at pH 7.6 and 2.0 mM cysteine were prepared. These samples were treated with 1 μL of DMSO or 1 μL of a 10 mM LN5P45 stock solution in DMSO (140 μM final concentration) and incubated for 30 min at room temperature. Samples were then diluted 3-fold with water and analyzed by mass spectrometry by injecting 1 μL into a Waters XEVO-G2 XS Q-TOF mass spectrometer equipped with an electrospray ion source in positive mode (capillary voltage 1.2 kV, desolvation gas flow 900 L/h, T = 60 °C) with a resolution of R = 26 000. Samples were run using two mobile phases: (A) 0.1% formic acid in water and (B) 0.1% formic acid in CH_3CN on a Waters Acquity UPLC protein BEH C4 column [300 Å, 1.7 μm (2.1 × 50 mm^2), flow rate = 0.5 mL/min, run time = 14.00 min, column T = 60 °C, and mass detection 200−2500 Da]. Gradient: 2−100% B. Data processing was performed using Waters MassLynx mass spectrometry software 4.1, and ion peaks were deconvoluted using the built-in MaxEnt1 function.

OTUB2 crystallization

For crystallization the covalent LN5P45-OTUB2 complex was generated by incubating 40 μM purified OTUB2 with a five-fold excess of the inhibitor for 1 hour at 37°C in GF buffer (50 mM Tris pH7.5, 100 mM NaCl, 2 mM TCEP). The formation of the covalent complex was confirmed using LCMS (Xevo) before being applied to a Superdex75 16/60 (GE Healthcare) gel filtration column equilibrated in GF buffer. The peak fractions containing the complex were concentrated to 24.5 mg mL-1 and flash frozen in liquid N2 awaiting crystallization.

Sitting drops were set up in a 1:1 ratio with the mother liquor and crystals appeared after several days in conditions with 0.1 M HEPES pH 8.0, 8-20% (v/v) isopropanol and 10-16% PEG 4000. Single crystals were frozen in mother liquor and 30% ethylene glycol as cryoprotectant and shipped to Diamond Light Source (DLS, United Kingdom) for diffraction.

Crystal data collection and structure determination

Crystals were diffracted at beamline I04-1 at Diamond and the resulting data sets were processed with DIALS [2] using the DLS computing grid. The CCP4 program suite [3] was used: first data reduction with Aimless [4], followed by molecular replacement using PHASER [5] with OTUB2 from PDB entry 5QIO as a search model. Iterative cycles of refinement using REFMAC [6] and model building with COOT [7] were performed before placing the LN5P45 inhibitor in the remaining density. Restraints for the inhibitor were generated using the GRADE webserver (Global Phasing Ltd.) and used in further refinement. Data processing and refinement statistics are reported in Supplementary Table S1 and the final model will be deposited in the Protein Data Bank (PDB ID: ####).

Cell culture and reagents

HEK293T (ATCC), HeLa (ATCC) and bone metastatic (BM) MDA-MB-231 cells [8] (laboratory of Peter ten Dijke) were cultured in under standard conditions in Dulbecco's modified Eagle's medium (DMEM) (Gibco) supplemented with 8% FCS (Biowest) and 1% penicillin/streptomycin at 37 °C and 5% CO_2. All cell lines were tested for mycoplasma

contamination using MycoAlert™ Mycoplasma Detection Kit (Lonza, Catalog #: LT07-318) on a monthly basis.

For siRNA transfections, OTUB2 siRNA oligos were purchased from Dharmacon. siOTUB2 pool of 4 (siGENOME Cat# MQ-010983-01-0002), siOTUB2_P1 (Cat# D-010983-01), siOTUB2_P2 (Cat# D-010983-02), siOTUB2_P3 (Cat# D-010983-03), and siOTUB2_P4 (Cat# D-010983-04). Silencing was performed in BM MDA-MB-231 cells as follows: for 6-well plate format, 200 µL siRNA (500 nM stock) were incubated with 4 µL Dharmafect reagent 1 (Dharmacon) diluted in 196 µL medium without supplements (total volume of 200 µL transfection mix) with gentle shaking for 20 min at room temperature (RT). A total of 80,000 cells resuspended in 1.6 mL of growth medium were added to transfection mixes to a total volume of 2 mL per well and cultured for 3 days prior to further analysis.

For DNA transfections, HEK293T cells were seeded to achieve 50–60% confluence the following day and transfected using PEI (polyethylenimine, Polysciences Inc., Cat# 23966) as follows: 200 µL DMEM medium without supplements was mixed with DNA and PEI (1 mg/mL) with a ratio at 1:3 (eg: 1µg DNA : 3µL PEI), incubated at RT for 20 min, and added drop-wise to the cells for culturing for 24 h prior to further analysis. The reaction was scaled using the same component ratios as follows: 12-well plate-1µg DNA , 6-well plate-3µg DNA, 6 cm dish- 8ug DNA.

DNA constructs

GFP-OTUB2 WT and C51S mutant [9], HA-Ub [10], Flag-HA-OTUB2 WT (#22552, Addgene) [11], pOPINK-OTUB2 (#61421, Addgene) [12] constructs have been previously described.

For site-directed mutagenesis of OTUB2 K12R, K31R, K37R, K44R, K46R and K211R, the same protocol was used as before [13]. In brief, a PCR mixture containing GFP-OTUB2 WT template, mutation primers, Pfu buffer, dNTPs, Turbo Pfu Polymerase (Agilent), and MilliQ water up to 50 µL reaction volume was subjected to PCR amplification using the following program: 95 °C for 2 min (95 °C for 50 s; 60 °C for 1 min; 68 °C for 1 min/Kb)×18 cycles; 68 °C for 20 min; 4 °C forever. PCR products were digested with 1 µL DpnI (Thermo Fischer Scientific) for 2 h at 37 °C to remove methylated DNA template, then transformed into competent DH5α. All mutated constructs were verified by sequencing. For primer sequences refer to the table below. All primers were purchased from IDT.

Gene	usage	Forward primer (5' -> 3')	Reverse (5' -> 3')
OTUB2	K12R point mutation	GAAGAATGGATAGAATGTCACATCTTTCTGATATTAGGTTGAAAGATG	CATCTTTCAACCTAATATCAGAAAGATGTGACATTCTATCCATTCTTC
OTUB2	K31R point mutation	TGCTGAGTTCCTCGATTCTCCTCCGGTAAATCCTG	CAGGATTTACCGGAGGAGAATCGAGGAACTCAGCA
OTUB2	K37R point mutation	GATGGCGGTGAACCTTCTGCTGAGTTCCTCGAT	ATCGAGGAACTCAGCAGAAGGTTCACCGCCATC

OTUB2	K44R point mutation	CATCCCCTTTGGTCCTG CGGATGGCGGTG	CACCGCCATCCGCAGGA CCAAAGGGGATG
OTUB2	K46R point mutation	CCCATCCCCTCTGGTCT TGCGGATGGCGG	CCGCCATCCGCAAGACC AGAGGGGATGGG
OTUB2	K221R point mutation	GTAGTGGGATGTTCTA TAGAGCAGGTAAACGG AAGGGG	CCCCTTCCGTTTACCTGC TCTATAGAACATCCCAC TAC

Antibodies, purified enzymes, and chemical compounds

The following antibodies were used for detection of endogenous and overexpressed proteins by immunoblots: mouse anti-Ubiquitin (P4D1, Santa Cruz Biotechnology, 1:1000 dilution), mouse anti-HA (16B12, Enzo Lifesciences, 1:1000 dilution), rabbit anti-mGFP [14] (self-made, 1:1000 dilution), mouse anti-GAPDH (1D4, Enzo Lifesciences, 1:1000 dilution) or mouse anti-β-actin (clone AC-15, Sigma-Aldrich, 1:5000 dilution).

The following purified DUBs were in vitro substrate cleavage assay: OTUB1 (full-length, in-house stock [15]), OTUB2 (full-length, in-house stock [15]), GST-OTUD6B (full-length, Ubiquigent. # 64-0028-050), UCHL1 (full-length, in-house stock [8]), UCHL3 (full-length, in-house stock [16]), UCHL5 (full-length, in-house stock [15]), USP2 (full-length, isoform 4, Ubiquigent. # 64-0014-050), USP5 (full-length, Ubiquigent. # 64-0002-050), USP7 (full-length, in-house stock [15]), USP8 (full-length, Ubiquigent. # 64-0053-050), USP16 (full-length, isoform 3, in-house stock [15]).

The following chemical compounds were used for proteasome activity modulation: PD169316 (PD) (CAS Number: 152121-53-4, Sigma Aldrich), Win 62,577 (Win) (CAS Number: 138091-43-7, Sigma Aldrich), MG-132 (CAS Number: 1211877-36-9, Sigma Aldrich), Cycloheximide (CAS Number: 66-81-9, Sigma Aldrich)

Ub-based activity-based probe (Rhodamine-Ub-PA) labeling

The in-cell inhibition of OTUB2 was assessed by using DUB probe labelling assay [17]. In brief, cell pellets were resuspended in HR buffer (50 mM Tris-HCl, 5 mM MgCl2, 250 mM sucrose, 2 mM TCEP and a Protease inhibitor tablet (Roche), pH 7.4), and lysed by sonication (Bioruptor, Diagenode, high intensity for 10 minutes with an ON/OFF cycle of 30 seconds) at 4°C. 40 µg clarified cell lysate was labelled with Rhodamine-Ubiquitin-propargylamide probe (final concentration at 1µM) at 37 °C for 30 min. Reactions were stopped by the addition of LDS (lithium dodecyl sulfate) sample buffer (Invitrogen Life Technologies, Carlsbad, CA, USA) containing 2.5% β-mercaptoethanol, followed by boiling for 7 minutes.

SDS-PAGE, in-gel fluorescence scan, and immunoblotting

Samples were resolved on precast Bis-Tris NuPAGE Gels (Invitrogen, including 4-12%, and 10% for different samples) using MOPS buffer (Invitrogen Life Technologies, Carlsbad, CA, USA).

For fluorescence scan, labeled enzymes were visualized by in-gel fluorescence using a Typhoon FLA 9500 imaging system (GE Healthcare Life Sciences) (Rhodamine channel for probe, Cy5 channel for protein marker).

For immunoblotting, proteins were transferred to a nitrocellulose membrane (Protan BA85, 0.45 μm, GE Healthcare) at 300 mA for 3 hours. The membranes were blocked in 5% milk (skim milk powder, LP0031, Oxiod) in 1× PBS (P1379, Sigma-Aldrich), incubated with a primary antibody diluted in 5% milk in 0.1% PBS-Tween 20 (PBST) for overnight at cold room, washed three times for 5 min in 0.1% PBST, incubated with the secondary antibody diluted in 5% milk in 0.1% PBST for 1 hour, and washed three times again in 0.1% PBST. The signal was visualized using a LICOR Odyssey system. Intensity of bands was quantified using the Image Studio software.

Real-time Quantitative RT-PCR

The mRNA level change of endogenous OTUB2 was assessed by RT-qPCR as before [8]. In brief, total RNAs were extracted using the NucleoSpin RNA II kit (MACHEREY-NAGEL) following to the manufacturer instructions. 1ug of total RNA were reversely transcribed using RevertAid First Stand cDNA synthesis Kits (Thermo Fisher), and real-time quantitative PCR experiments were performed using SYBR Green (Promega) in CFX connect Real-Time PCR detection system (Bio-Rad). All the values for target gene expression were normalized to GAPDH. Primers are listed below. All the experiments were repeated in n=3 independent experiments.

Gene	usage	Forward primer (5' -> 3')	Reverse (5' -> 3')
OTUB2	qPCR	TTCTTCGGGACCATCCTGAAA	CCAGGTAGGAATAGCCCAAGG
GAPDH	qPCR	TGCACCACCAACTGCTTAGC	CTCATGACCACAGTCCATGCC

GFP-OTUB2 pulldown assays

To check the PTM on GFP-OTUB2, GFP trap pulldown assay was applied as before [13].HEK293T cells, transfected GFP-OTUB2 variants as indicated, were lysed in 300 μL lysis buffer 1 (50 mM Tris-HCl, pH 7.5, 150 mM NaCl, 0.5% Triton X-100, 10 mM N-methyl maleimide (general DUB inhibitor diluted in DMSO, freshly added) and protease inhibitors (Roche Diagnostics, EDTA-free, freshly added). Then, 100 μL lysis buffer 2 (100 mM Tris-HCl, pH 8.0, 1 mM EDTA, and 2% SDS) were added to the crude lysates; samples were sonicated (Fisher Scientific FB120 Sonic Dismembrator, 3 pulses, amplitude 40%) and SDS was subsequently diluted by bringing sample volume to 1 mL with lysis buffer 1. After centrifugation (20 min, 4 °C, 20,817× g), lysates were incubated with 6 μL GFP Trap Agarose (Chromotek) overnight at 4 °C. Beads were washed 5 times with lysis buffer 1, and denatured with sample buffer by heating at 95 °C for 7 min. Samples were subjected to 4-12% SDS-PAGE, gel samples either sliced for protein mass spectrometry detection, or transferred to Nitrocellulose membranes for immunoblots, as indicated.

For enhanced ubiquitination assay, HEK293T cells were co-transfected with GFP-OTUB2 variants and HA-Ub as indicated.

***In vitro* deubiquitination assay**

Ubiquitinated GFP-OTUB2 substrates were prepared from HEK293T cells. In brief, GFP-OTUB2 WT construct was transfected into HEK293T cells. At 24 h post transfection, cells were incubated with LN5P45 at 10 μM for 4 hours before harvesting. Cell lysates were subjected to GFP trap pulldown as above. The beads were washed 5 times with assay buffer (50mM Tris-HCl pH 7.4, 150 mM NaCl, 2 mM EDTA, 0.5 % NP40, 5mM TCEP), then equally aliquoted into PCR tubes, and the liquids were removed. The beads mixture were incubated with recombinant DUBs at 37 °C for 2 hours. recombinant OTUB2, OTUB1, GST-OTUD6B, UCHL1, UCHL3 and UCHL5 were added at final concentration of 2.5 μM; USP2, USP5, USP7, USP8 and USP16 full-length protein were added with a total amount of 1 μg. The reaction was stopped by boiling with LDS sample buffer as described above.

For inactivating recombinant OTUB2, recombinant OTUB2 was diluted with assay buffer into 2.5uM, and incubated with LN5P45 (final conc. 200μM) for 15min at room temperature.

Protein mass spectrometry of gel slices

For MS analysis, gel slices were subjected to reduction with dithiothreitol, alkylation with iodoacetamide and in-gel trypsin digestion using a Proteineer DP digestion robot (Bruker). Tryptic peptides were extracted from the gel slices, lyophilized, dissolved in 95/3/0.1 v/v/v water/acetonitril/formic acid and subsequently analyzed by on-line C18 nanoHPLC MS/MS with a system consisting of an Easy nLC 1000 gradient HPLC system (Thermo, Bremen, Germany),), and a LUMOS mass spectrometer (Thermo). Samples were injected onto a homemade precolumn (100 μm × 15 mm; Reprosil-Pur C18-AQ 3 μm, Dr. Maisch, Ammerbuch, Germany) and eluted via a homemade analytical nano-HPLC column (30 cm × 50 μm; Reprosil-Pur C18-AQ 3 um). The gradient was run from 10% to 40% solvent B (20/80/0.1 water/acetonitrile/formic acid (FA) v/v) in 30 min. The nano-HPLC column was drawn to a tip of ~5 μm and acted as the electrospray needle of the MS source. The LUMOS mass spectrometer was operated in data-dependent MS/MS mode for a cycle time of 3 seconds, with a HCD collision energy at 32 V and recording of the MS2 spectrum in the orbitrap. In the master scan (MS1) the resolution was 120,000, the scan range 400-1500, at an AGC target of 400,000 @maximum fill time of 50 ms. Dynamic exclusion after n=1 with exclusion duration of 10 s. Charge states 2-5 were included. For MS2 precursors were isolated with the quadrupole with an isolation width of 1.2 Da. First mass was set to 110 Da. The MS2 scan resolution was 30,000 with an AGC target of 50,000 @maximum fill time of 60 ms.

Profiling of LN5P45-reactive cysteines by SLC-ABPP

SLC-ABPP profiling was performed as described before [1]. In short: HeLa cells, transfected with GFP or GFP-OTUB2 WT with PEI reagent for 24 hours, were grown to 80% confluence and incubated with either DMSO or 10 μM LN5P45 for 4 h in complete medium. Cells were harvested, lysed by sonication in ice-cold PBS and centrifuged at 15.000 RPM for 2 min to remove cell debris. Protein concentrations were then determined by BCA Gold protein assay. Proteomes were normalized to 1 mg /ml in 100 μL for each sample.

Each DMSO- and LN5P45-treated proteome was labeled with 500 µM DBIA probe for 1 hour in the dark at room temperature (RT). Excess DBIA, along with disulfide bonds, were quenched and reduced using 5 mM dithiothreitol for 30 min in the dark at RT. Reduced disulphide bonds were alkylated using 20 mM iodoacetamide for 30 min in the dark at RT. Proteins were precipitated using chloroform/methanol, and re-solubilized in 40 mM HEPES pH 8.4 and digested using TPCK treated trypsin and endoLysC (1:12.5 enzyme/protein ratio) overnight at 37 °C. Digested peptides were labeled using TMTpro16-plex reagents in a 1:4 ratio by mass (peptides:TMT reagents) for 1 h at RT. Excess TMT reagent was quenched with 5 µL 6% hydroxylamine for 15 min at RT. Next, samples were mixed 1:1 across all TMT channels and the pooled sample was dried using a Speedvac.

Dried samples were reconstituted in 1ml PBS, and enriched by Pierce streptavidin magnetic beads (Catalog number: 88816, Thermo Scientific™) by rotating end-over-end overnight at 4 °C. Nonspecific binding peptides were washed using the following procedure: 3 ×1 ml of PBS pH 7.4, 2 × 1 ml of PBS with 0.1% SDS pH 7.4, and 3 × 1 ml of HPLC-grade water. DBIA probe-containing peptides were eluted using 700 µL of 50% acetonitrile with 0.1% TFA, dried using a Speedvac and desalted using a mini-SPE column (10% sorbent material of a Waters, OASIS 1cc HLB 30 mg cartridge). Column was washed with 200 µL 90% acetonitrile and 3x 200 µL 10 mM NH_4HCO_3 pH 8.4. Dried sample was dissolved in 200 µL 10 mM NH_4HCO_3 pH 8.4, loaded onto the column, washed 3x with 200 µL 10 mM NH_4HCO_3 pH 8.4 and eluted into 3 fractions with 150 µL each of 10%, 20% and 50% acetonitrile (in 10 mM NH_4HCO_3). Sample was re-dried using a Speedvac.

Mass spectrometry of SLC-ABPP

Peptides were lyophilized, dissolved in 0.1% formic acid and subsequently analyzed by on-line C18 nanoHPLC MS/MS with a system consisting of an Ultimate3000nano gradient HPLC system (Thermo, Bremen, Germany), and an Exploris480 mass spectrometer (Thermo). Fractions were injected onto a cartridge precolumn (300 µm × 5 mm, C18 PepMap, 5 um, 100 A, and eluted via a homemade analytical nano-HPLC column (50 cm × 75 µm; Reprosil-Pur C18-AQ 1.9 um, 120 A (Dr. Maisch, Ammerbuch, Germany). The gradient was run from 2% to 40% solvent B (20/80/0.1 water/acetonitrile/formic acid (FA) v/v) in 120 min. The nano-HPLC column was drawn to a tip of ~10 µm and acted as the electrospray needle of the MS source. The mass spectrometer was operated in data-dependent MS/MS mode for a cycle time of 3 seconds, with a HCD collision energy at 36 V and recording of the MS2 spectrum in the orbitrap, with a quadrupole isolation width of 1.2 Da. In the master scan (MS1) the resolution was 120,000, the scan range 350-1600, at standard AGC target @maximum fill time of 50 ms. A lock mass correction on the background ion m/z=445.12 was used. Precursors were dynamically excluded after n=1 with an exclusion duration of 45 s, and with a precursor range of 20 ppm. Charge states 2-5 were included. For MS2 the first mass was set to 110 Da, and the MS2 scan resolution was 45,000 at an AGC target of 200% with a maximum fill time set to auto.

Protein mass spectrometry data analysis

In a post-analysis process, raw data were first converted to peak lists using Proteome Discoverer version 2.4 (Thermo Electron), and then submitted to the Uniprot Homo sapiens minimal database (20205 entries), using Mascot v. 2.2.04 (www.matrixscience.com) for protein identification. Mascot searches were done with 10 ppm and 0.02 Da deviation for precursor and fragment mass, respectively, and the enzyme

trypsin was specified, up to two missed cleavages were allowed for gel slices and three missed cleavages for SLC-ABPP. For gel slices, methionine oxidation and ubiquitination (GG) on lysine were set as a variable modification; carbamidomethyl on Cys was set as a fixed modification. For SLC-ABPP, methionine oxidation, Acetyl (protein N-term) and DBIA on Cys were set as a variable modification. Carbamidomethyl on Cys and TMTpro on Lys and N-term were set as a fixed modification. Peptides with an FDR<1% in were accepted. Abundance ratios were calculated by dividing the inhibitor-treated channels with the DMSO-treated channels.

Statistical analysis

Immunoblot protein bands were quantified using ImageJ software (NIH). quantification Statistical evaluations report on Student's t test (two-tailed distribution) with $*p < 0.05$, $**p < 0.01$, and $***p < 0.001$, NS: not significant). All error bars correspond to the mean ± SD or mean ± S.E.M (qPCR data only)

REFERENCES

1. Kuljanin, M., et al., *Reimagining high-throughput profiling of reactive cysteines for cell-based screening of large electrophile libraries.* Nat Biotechnol, 2021. **39**(5): p. 630-641.
2. Winter, G., et al., *DIALS: implementation and evaluation of a new integration package.* 2018. **74**(2): p. 85-97.
3. Winn, M.D., et al., *Overview of the CCP4 suite and current developments.* 2011. **67**(4): p. 235-242.
4. Evans, P.R. and G.N.J.A.C.S.D.B.C. Murshudov, *How good are my data and what is the resolution?* 2013. **69**(7): p. 1204-1214.
5. McCoy, A.J., et al., *Phaser crystallographic software.* 2007. **40**(4): p. 658-674.
6. Murshudov, G.N., et al., *REFMAC5 for the refinement of macromolecular crystal structures.* 2011. **67**(4): p. 355-367.
7. Emsley, P. and K.J.A.c.s.D.b.c. Cowtan, *Coot: model-building tools for molecular graphics.* 2004. **60**(12): p. 2126-2132.
8. Liu, S., et al., *Deubiquitinase Activity Profiling Identifies UCHL1 as a Candidate Oncoprotein That Promotes TGFbeta-Induced Breast Cancer Metastasis.* Clin Cancer Res, 2020. **26**(6): p. 1460-1473.
9. Ekkebus, R., et al., *On terminal alkynes that can react with active-site cysteine nucleophiles in proteases.* J Am Chem Soc, 2013. **135**(8): p. 2867-70.
10. Berlin, I., H. Schwartz, and P.D. Nash, *Regulation of epidermal growth factor receptor ubiquitination and trafficking by the USP8·STAM complex.* J Biol Chem, 2010. **285**(45): p. 34909-21.

11. Sowa, M.E., et al., *Defining the human deubiquitinating enzyme interaction landscape.* Cell, 2009. **138**(2): p. 389-403.

12. Mevissen, T.E.T., et al., *OTU deubiquitinases reveal mechanisms of linkage specificity and enable ubiquitin chain restriction analysis.* Cell, 2013. **154**(1): p. 169-184.

13. Sapmaz, A., et al., *USP32 regulates late endosomal transport and recycling through deubiquitylation of Rab7.* Nat Commun, 2019. **10**(1): p. 1454.

14. van der Kant, R., et al., *Late endosomal transport and tethering are coupled processes controlled by RILP and the cholesterol sensor ORP1L.* J Cell Sci, 2013. **126**(Pt 15): p. 3462-74.

15. Mons, E., et al., *Exploring the Versatility of the Covalent Thiol-Alkyne Reaction with Substituted Propargyl Warheads: A Deciding Role for the Cysteine Protease.* J Am Chem Soc, 2021. **143**(17): p. 6423-6433.

16. van Tilburg, G.B.A., et al., *K27-Linked Diubiquitin Inhibits UCHL3 via an Unusual Kinetic Trap.* Cell Chem Biol, 2021. **28**(2): p. 191-201.e8.

17. Resnick, E., et al., *Rapid covalent-probe discovery by electrophile-fragment screening.* 2019. **141**(22): p. 8951-8968.

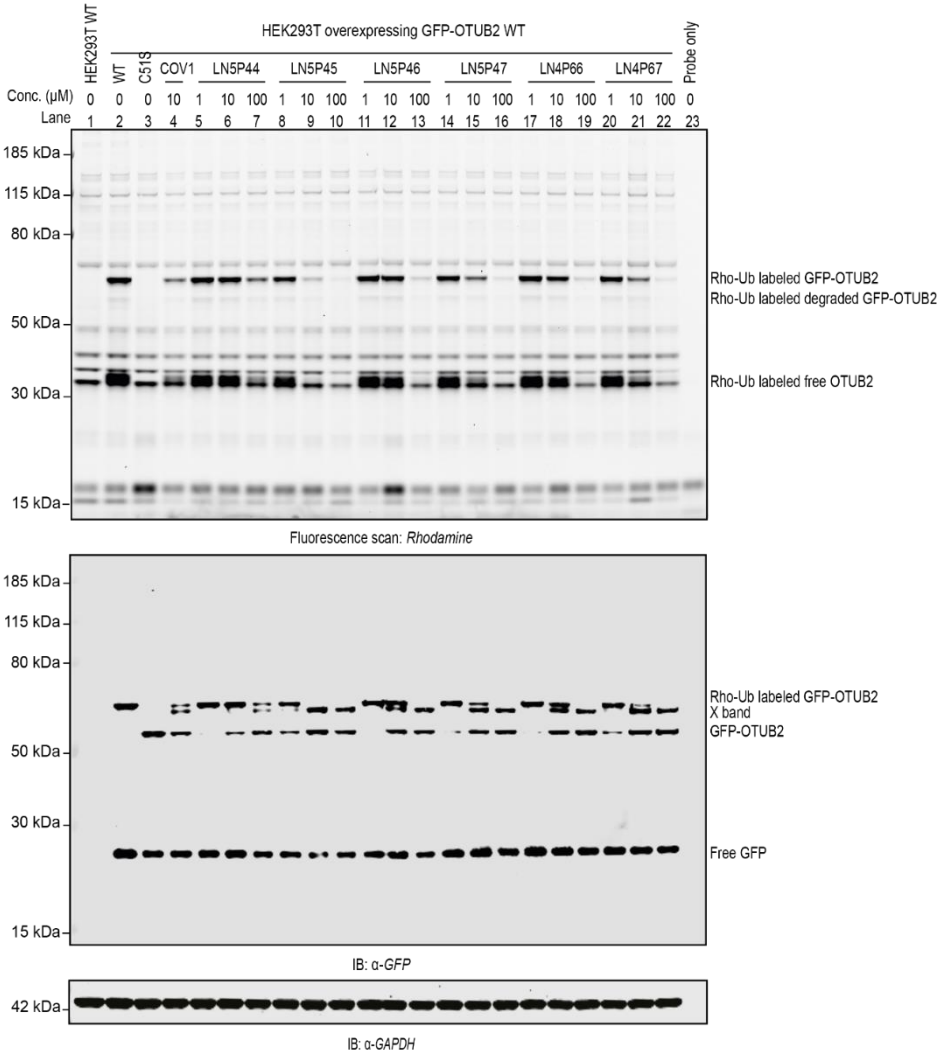

Supplementary Figure 1. Full image of Figure 1D. Inhibition of GFP-OTUB2 by the indicated compounds in HEK293T cells. GFP-OTUB2 (WT or catalytic dead mutant C51S) was transiently transfected in HEK293T cells. After 24 hours, cells were treated with indicated inhibitors at indicated concentrations for 4 hours. Cell lysates were incubated with Rho-Ub-PA probe, and subjected to SDS-PAGE, gel fluorescence scanning, and immunoblotting. Top: fluorescence scan of Rho-Ub-PA probe labelled DUBs. Middle: anti-GFP immunoblot data corresponding to probe labelled and unlabeled GFP-OTUB2 (An extra band was annotated as "X band", see results in Figure 4). Bottom: anti-GAPDH immunoblot data validating equal loading of each sample. The overexpressed GFP-OTUB2 in HEK293T cells can be partially degraded into a smaller product and free OTUB2. The labeling bands reduced by inhibitors correspond to GFP-OTUB2, partially degraded GFP-OTUB2 (between 50 and 80 kDa) and free OTUB2 cleaved from GFP-OTUB2 (just above 30 kDa).

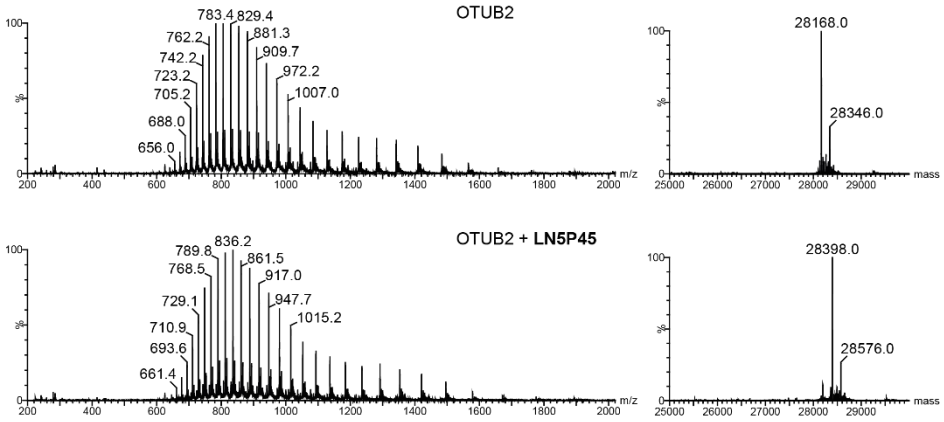

Supplementary Figure 2. MS analysis of covalent complex formation between OTUB2 and LN5P45 inhibitor, corresponding to Figure 2B. Deconvoluted mass is shown on the right.

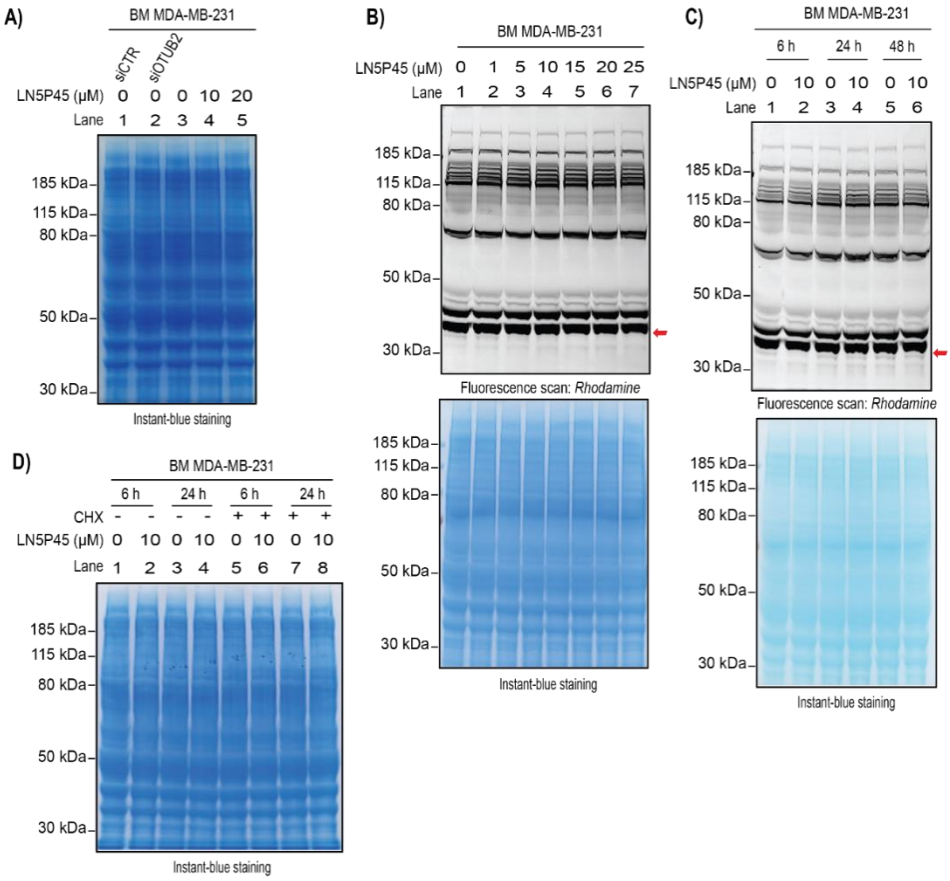

Supplementary Figure 3. Full fluorescence scans and instant-blue stained loading controls. (A) Instant-blue stained loading control for Figure 3A. (B) Full image of fluorescence scan with normal exposure, and Instant-blue stained loading control for Figure 3C. (C) Full image of fluorescence scan with normal exposure, and Instant-blue stained loading control for Figure 3D. (D) Instant-blue stained loading control for Figure 8B.

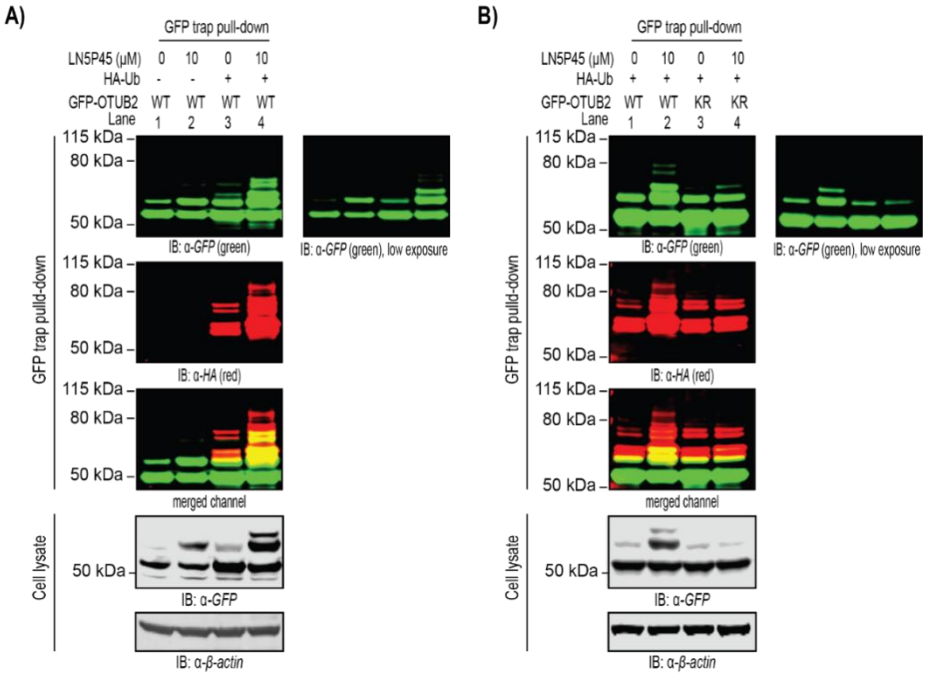

Supplementary Figure 4. Confirmation of ubiquitination of GFP-OTUB2 by HA-ubiquitin overexpression in HEK 293T cells. (A) Ubiquitination on GFP-OTUB2 demonstrated by overexpression of HA-Ub. GFP-OTUB2 WT pulled down from HEK293T cells co-expressing empty vector or HA-Ub, and inhibitor-treated for 4 hours or non-treated, was assessed by immunoblotting against the HA and GFP tags. (B) K31R mutation abolishes the inhibitor-induced enhancement of ubiquitination on GFP-OTUB2. GFP-OTUB2 WT or K31R mutant (KR) were co-expressed with HA-Ub and analysed as described under (A).

Supplementary Table 3. Data processing and refinement statistics for the OTUB2-LN5P45 cocrystal structure.

	OTUB2 +LN5P45
Crystallization conditions	17% (v/v) Isopropanol, 16% (w/v) PEG-4000, 0.1M HEPES pH 8.0
PDB accession code	Dataset F16 (submission pending)
Space group	P21
Cell dimensions	
a (Å)	47.4
b (Å)	45.4
c (Å)	57.6
α (°)	90
β (°)	96.2
γ (°)	90
Processing statistics	
Resolution (Å) Outer shell (Å)	57.28-1.56 1.58-1.56
Beamline	DLS I04-1
Wavelength (Å)	0.99 (!!!)
Observed reflections	103468 (3108)
Unique reflections	34151 (1480)
Rpim	0.046 (1.020)
CC(1/2)	0.999 (0.333)
Multiplicity	3.0 (2.1)
Completeness	97.3 (87.2)
Mean (I/σ(I))	9.5 (0.8)
Refinement statistics	
Monomers in ASU	1
No of protein atoms	0
Rwork	0.190
Rfree	0.229
RMSD from ideality	
Bond lengths (Å)	0.012
Bond angles (°)	1.780
Chiral volume (Å3)	0.091
Ramachandran plot	
Favoured (%)	96.4%
Disallowed (%)	0.9%
Average B-values (Å2)	-